Cooperative Reactivity in the Interactions of X-H Bonds with a Zirconium-Iridium Bridging Imido Complex

Anne M. Baranger and Robert G. Bergman*

Contribution from the Department of Chemistry, University of California, Berkeley, California 94720

*Received November 22, 1993**

Abstract: We report the synthesis of the first early-late heterobimetallic bridging imido complex $Cp_2Zr(\mu\text{-N-}t\text{-Bu})$-IrCp* (**1**). Complex **1** was synthesized in 65% yield by the sequential addition of *n*-BuLi and Cp*IrN-*t*-Bu to Cp_2ZrCl_2 and was characterized by an X-ray diffraction study. The Ir-Zr bond distance was found to be 2.598(2) Å, and the Ir-N (1.887(13) Å) and Zr-N (2.084(13) Å) bond distances are comparable to those observed in analogous homonuclear imido dimers. Imido complex **1** was found to undergo addition of both polar (N-H, O-H, S-H) and nonpolar (H-H, Si-H, C-H) X-H bonds across the Ir-Zr bond. For example, the reaction of imido complex **1** with *p*-toluidine resulted in the formation of $Cp_2Zr(NHAr)(\mu\text{-N-}t\text{-Bu})(\mu\text{-H})$IrCp* (**2**, 60% yield), the addition of *p*-cresol gave $Cp_2Zr(OAr)$-$(\mu\text{-N-}t\text{-Bu})(\mu\text{-H})$IrCp* (**3a**, 56% yield), the addition of *tert*-butyl alcohol led to $Cp_2Zr(O\text{-}t\text{-Bu})(\mu\text{-N-}t\text{-Bu})(\mu\text{-H})$IrCp* (**3b**, 74% yield), and the addition of acetone yielded $Cp_2Zr(OC(CH_2)CH_3)(\mu\text{-N-}t\text{-Bu})(\mu\text{-H})$IrCp* (**4**, 72% yield). Complexes **2** and **3a** were characterized by X-ray crystallography. The addition of *p*-thiocresol yielded two products, **5a** and **5b**. The major product was found to be spectroscopically similar to the *p*-toluidine, *p*-cresol, *tert*-butyl alcohol, and acetone addition products, suggesting a similar formulation ($Cp_2Zr(SAr)(\mu\text{-N-}t\text{-Bu})(\mu\text{-H})$IrCp*). Addition of H_2S to **1** resulted in formation of the bridging sulfido complex $Cp_2Zr(\mu\text{-N-}t\text{-Bu})(\mu\text{-S})$IrCp* (**6**, 45% yield), presumably by a similar X-H addition followed by elimination of H_2. The addition of diethylphosphine and cyclohexylphosphine to imido complex **1** resulted in the unusual insertion of phosphide (PR_2) into the Ir-N rather than the Ir-Zr bond to give $Cp_2Zr(\mu\text{-N}(t\text{-Bu})PEt_2)$Ir(H)Cp* (**8a**, 63% yield) and $Cp_2Zr(\mu\text{-N}(t\text{-Bu})PHCy)$Ir(H)Cp* (**8b**, 50% yield). An X-ray diffraction study was performed on **8a**, which revealed that the Ir-Zr bond distance was 2.642(1) Å, comparable to that in imido complex **1**. The *tert*-butoxide complex **3b** reacted with MeOTf to give $CpZr(O\text{-}t\text{-Bu})(OTf)(\mu\text{-H})$-$(\mu\text{-N-}t\text{-Bu})$IrCp* (**11**, 62% yield), a product resulting from the replacement of a single Zr-bonded Cp ligand with a triflate ligand. An X-ray diffraction study confirmed that the triflate ion was covalently bound to zirconium. The addition of trimethylphosphine to the *tert*-butoxide complex **3b** resulted in reductive elimination of the imido and hydrido bridges to give $Cp_2Zr(O\text{-}t\text{-Bu})(NH\text{-}t\text{-Bu})$ (**12**, 58% yield) and $Cp^*Ir(PMe_3)_2$ (84% yield). The addition of H_2 to **1** resulted in the reversible addition of the H-H bond across the Ir-Zr bond to form $Cp_2Zr(H)(\mu\text{-N-}t\text{-Bu})(\mu$-H)IrCp* (**9a**, 69% yield). The terminal and bridging hydrides underwent exchange with each other and with excess H_2. Addition of $MePhSiH_2$ to **1** resulted in $Cp_2Zr(SiHMePh)(\mu\text{-N-}t\text{-Bu})(\mu\text{-H})$IrCp* (**10**), a product analogous to that resulting from H_2 addition.

Introduction

The synthesis and reactivity of early-late heterobimetallic complexes have been the focus of numerous studies.[1-20] Interest in these complexes stems from the possibility of utilizing the complementary reactivities of the early and late transition metals in reactions with organic substrates. This is often referred to as "cooperative reactivity". The electron-poor early transition metal and the electron-rich late transition metal are likely to create an ideal environment for heterolytic bond cleavage of polar substrates. Although many early-late heterobimetallic complexes have been prepared, few exhibit cooperative reactivity with organic substrates.[2-9] In most cases, the observed chemistry takes place at a single metal center because the metal centers are not proximate enough to allow cooperative chemistry. In addition, the late transition metal is often more reactive due to electronic or steric saturation of the early metal center. Only a few reactions that take place at the late transition metal have been shown to be affected by the early transition metal,[2,4-6,9] and even fewer cases of direct participation by both metal centers in a reaction with an organic substrate have been observed.[3,7,8]

Another reason for the interest in early-late heterobimetallic complexes is their applications as models for early metal oxide supports which exhibit strong metal support interactions (SMSI).[21,22] SMSI cause group VIII metals supported on titania and

* Abstract published in *Advance ACS Abstracts,* April 1, 1994.

(1) For a review of early-late heterobimetallic complexes, see: Stephan, D. W. *Coord. Chem. Rev.* **1989**, *95*, 41.
(2) Hostetler, M. J.; Butts, M. D.; Bergman, R. G. *J. Am. Chem. Soc.* **1993**, *115*, 2743.
(3) Ferguson, G. S.; Wolczanski, P. T.; Párkányi, L.; Zonnevylle, M. C. *Organometallics* **1988**, *7*, 1967.
(4) Gelmini, L.; Stephan, D. W. *Organometallics* **1988**, *7*, 849.
(5) Choukroun, R.; Dahan, F.; Gervais, D.; Rifaï, C. *Organometallics* **1990**, *9*, 1982.
(6) Choukroun, R.; Gervais, D.; Jaud, J.; Kalck, P.; Senocq, F. *Organometallics* **1986**, *5*, 67.
(7) Casey, C. P. *J. Organomet. Chem.* **1990**, *400*, 205.
(8) Ozawa, F.; Park, J. W.; Mackenzie, P. B.; Schaefer, W. P.; Henling, L. M.; Grubbs, R. H. *J. Am. Chem. Soc.* **1989**, *111*, 1319.
(9) Senocq, F.; Randrianalimanana, C.; Thorez, A.; Kalck, P.; Choukroun, R.; Gervais, D. *J. Chem. Soc., Chem. Commun.* **1984**, 1376.
(10) Steffey, B. D.; Vites, J. C.; Cutler, A. R. *Organometallics* **1991**, *10*, 3432.
(11) Sartain, W. J.; Selegue, J. P. *Organometallics* **1989**, *8*, 2153.
(12) Katti, K. V.; Cavell, R. G. *Organometallics* **1991**, *10*, 539.
(13) Erker, G. *Polyhedron* **1988**, *7*, 2451.
(14) Casey, C. P.; Askham, F. R.; Petrovich, L. M. *J. Organomet. Chem.* **1990**, *387*, C31.
(15) Bullock, R. M.; Lemke, F. R.; Szalda, D. J. *J. Am. Chem. Soc.* **1990**, *112*, 3244.
(16) Bruno, J. W.; Huffman, J. C.; Green, M. A.; Caulton, K. G. *J. Am. Chem. Soc.* **1984**, *106*, 8310.
(17) Bullock, R. M.; Casey, C. P. *Acc. Chem. Res.* **1987**, *20*, 167.
(18) Baxter, S. M.; Ferguson, G. F.; Wolczanski, P. T. *J. Am. Chem. Soc.* **1988**, *110*, 4231.
(19) Baker, R. T.; Fultz, W. C.; Marder, T. B.; Williams, I. D. *Organometallics* **1990**, *9*, 2357.
(20) Glassman, T. E.; Liu, A. H.; Schrock, R. R. *Inorg. Chem.* **1991**, *30*, 4723.
(21) *Strong Metal-Support Interactions*; ACS Symposium Series 298; American Chemical Society: Washington, DC, 1985.

0002-7863/94/1516-3822$04.50/0

other early metal oxides to be more active toward catalytic hydrogenation of carbon monoxide. Little is known about the chemical origin of SMSI, but it is postulated that there is an interaction between Ti(III) and the oxygen of carbon monoxide and between the group VIII metal and the carbon of carbon monoxide.[21,22] This interaction would require a close Ti–M contact. The reactivity of early–late heterobimetallic complexes that contain metal–metal bonds might provide insight into the mechanism of SMSI.

We wish to report here the synthesis and reactivity of the early–late bridging imido complex **1** ($Cp_2Zr(\mu\text{-N-}t\text{-Bu})IrCp^*$, $Cp^* = C_5Me_5$).[23] To our knowledge complex **1** is the first example of an early–late heterobimetallic bridging imido complex and contains the first structurally characterized Ir–Zr bond. Imido complex **1** is ideal for cooperative reactivity studies because it contains two unsaturated and thus potentially reactive metal centers. In addition, the metal–metal bond provides a site for reactivity which must necessarily involve both metal centers, while the imido bridge can prevent dissociation when the metal–metal bond is broken. We have examined the reactivity of **1** with both polar and nonpolar X–H bonds, and we have investigated the subsequent reactivity of the products.

Most of the reactions we have observed with imido complex **1** have involved additions of organic reagents across the Ir–Zr bond. Although there has not been an extensive study of the reactivity of early–late heterobimetallic bonds, there have been extensive studies of the reactions of metal–metal bonds in cluster compounds, compounds containing metal–metal multiple bonds, and bimetallic compounds.[24–34] Most addition reactions of these complexes have been with H_2, HX, X_2, or MeI. There have been more limited studies on the addition of alcohols[27] and phosphines[34] and almost none involving amines or carbon acids.

Results

Synthesis of the Heterobimetallic Imido Complex 1. The addition of 2 equiv of *n*-BuLi to Cp_2ZrCl_2 at –30 °C in THF followed by treatment with $Cp^*IrN\text{-}t\text{-}Bu$ produced the heterobimetallic bridging imido complex $Cp_2Zr(\mu\text{-N-}t\text{-Bu})IrCp^*$ (**1**) in 2 days at room temperature (eq 1). The addition of *n*-BuLi to

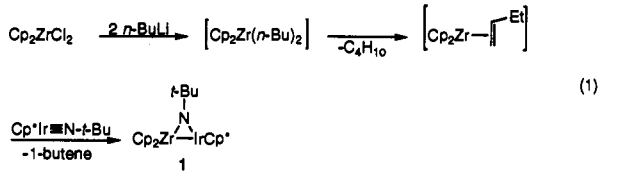

(1)

Cp_2ZrCl_2 at low temperature has been shown to proceed via the bis-*n*-butyl complex ($Cp_2Zr(n\text{-}Bu)_2$), followed by β-elimination to form the butene complex ($Cp_2Zr(CH_2{=}CHCH_2CH_3)$).[35] Imido complex **1** was isolated as dark brown crystals in 65% yield by cooling a diethyl ether solution to –30 °C. The structure of this compound was confirmed by an X-ray crystallographic study of crystals grown under these conditions. An ORTEP drawing is shown in Figure 1. Crystal parameters are given in Table 1, data collection parameters in Table 2, selected bond lengths in Table 3, and selected bond angles in Table 4. The Ir–Zr bond length of 2.598(2) Å and the acute Ir–N–Zr angle of 81.6(5)° are consistent with the presence of a metal–metal bond. Complex **1** is planar at nitrogen, indicating the donation of the lone pair into empty orbitals on at least one of the metal centers. The Zr–N bond length of 2.084(13) Å is normal for zirconium bridging imido dimers,[36–41] and the Ir–N bond length (1.887(13) Å) is comparable to that of the related bridging iridium imide Cp^*Ir-

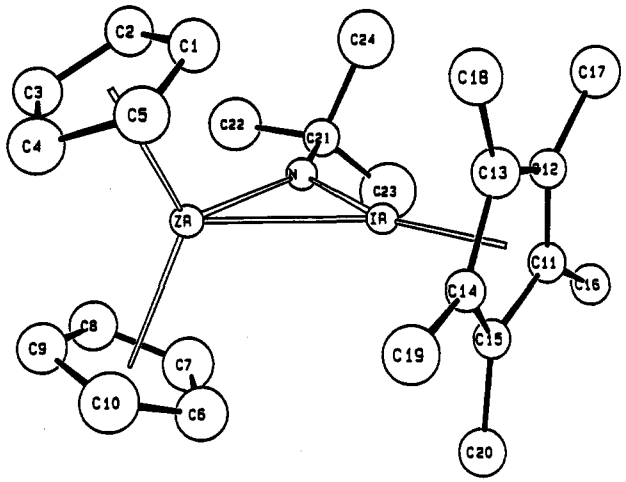

Figure 1. ORTEP diagram of $Cp_2Zr(\mu\text{-N-}t\text{-Bu})IrCp^*$ (**1**). The hydrogen atoms were not located.

Table 1. Crystal Parameters for Complexes **1**, **2**, and **3a**

	1[a,b]	**2**[b,c,d]	**3a**[b,e]
empirical formula	$C_{24}H_{34}IrNZr$	$C_{38}H_{50}IrN_2Zr$	$C_{31}H_{42}IrNOZr$
formula wt (amu)	620.0	818.3	728.1
crystal size	0.15 × 0.15 × 0.25	0.12 × 0.20 × 0.35	0.25 × 0.30 × 0.40
space group	*Cc*	*Pbca*	$P2_12_12_1$
a (Å)	14.476(5)	13.824(4)	10.901(3)
b (Å)	15.406(3)	23.470(4)	14.178(4)
c (Å)	10.398(3)	21.271(5)	19.133(7)
β (deg)	96.93(2)	90.0	90.0
V (Å^3)	2302.0(20)	6901.2(47)	2957.2(27)
Z	4	8	4
d_{calc} (g cm^{-3})	1.79	1.57	1.64
μ_{calc} (cm^{-1})	62.1	41.6	48.5

[a] Unit cell parameters and their esd's were derived by a least-squares fit to the setting angles of the unresolved Mo Kα components, 25 reflections with 2θ equal to 24°. [b] In this and all subsequent tables the esd's of all parameters are given in parentheses to the right of the least significant digit(s) of the reported value. [c] Unit cell parameters and their eds's were derived by a least-squares fit to the setting angles of the unresolved Mo Kα components, 24 reflections with 2θ between 22 and 26°. [d] Complex **2** cocrystallized with 1 equiv of toluene. [e] Unit cell parameters and their esd's were derived by a least-squares fit to the setting angles of the unresolved Mo Kα components, 22 reflections with 2θ equal to 26°.

(22) Tauster, S. J. *Acc. Chem. Res.* **1987**, *20*, 389.
(23) Portions of the work reported here have been published earlier in communication form: Baranger, A. M.; Hollander, F. J.; Bergman, R. G. *J. Am. Chem. Soc.* **1993**, *115*, 7890.
(24) For a review of heteronuclear bonds between transition metals, see: Roberts, D. A.; Geoffrey, G. L. In *Comprehensive Organometallic Chemistry*; Wilkinson, G., Stone, F. G. A., Abel, E. W., Eds.; Pergamon Press: New York, 1982; Vol. 6, pp 763–877.
(25) For a review of reactions of homonuclear metal–metal bonds in metal clusters, see: Vahrenkamp, H. *Adv. Organomet. Chem.* **1983**, *22*, 169.
(26) For a review of reactions of metal–metal multiple bonds, see: Cotton, F. A. *J. Chem. Ed.* **1983**, *60*, 713.
(27) Chisholm, M. H. *Polyhedron* **1986**, *5*, 25.
(28) Curtis, M. D. *Polyhedron* **1987**, *6*, 759.
(29) Messerle, L. *Chem. Rev.* **1988**, *99*, 1229.
(30) Lu, K. L.; Lin, Y. C.; Wang, Y. *Organometallics* **1990**, *9*, 1320.
(31) Finke, R. G.; Gaughan, G.; Pierpont, C.; Noordik, J. H. *Organometallics* **1983**, *2*, 1481.
(32) Bruno, G.; Schiavo, S. L.; Coleman, A. W.; Eadie, D. T.; Stobart, S. R. *J. Am. Chem. Soc.* **1982**, *104*, 922.
(33) Biddulph, M. A.; Davis, R.; Wilson, F. I. C. *J. Organomet. Chem.* **1990**, *387*, 277.
(34) Baker, R. T.; Calabrese, J. C.; Glassman, T. E. *Organometallics* **1988**, *7*, 1889.
(35) Negishi, E.; Holmes, S. J.; Tour, J. M.; Miller, J. A.; Cederbaum, F. E.; Swanson, D. R.; Takahashi, T. *J. Am. Chem. Soc.* **1989**, *111*, 3336.
(36) Wielstra, Y.; Meetsma, A.; Gambarotta, S.; Khan, S. *Organometallics* **1990**, *9*, 876.
(37) Walsh, P. J.; Hollander, F. J.; Bergman, R. G. *J. Am. Chem. Soc.* **1988**, *110*, 8729.
(38) Nugent, W. A.; Harlow, R. L. *Inorg. Chem.* **1979**, *18*, 2030.
(39) Fryzuk, M. D.; Haddad, T. S.; Rettig, S. J. *J. Am. Chem. Soc.* **1990**, *112*, 8185.
(40) Arvanitis, G. M.; Smegal, J.; Meier, I.; Wong, A. C. C.; Schwartz, J.; Engen, D. V. *Organometallics* **1989**, *8*, 2717.

Table 2. Data Collection Parameters for Complexes **1**, **2**, and **3a**

	1	2	3a
temp (°C)	−110	−106	−99
rflcns measd	$\pm h, +k, +l$	$+h, +k, +l$	$+h, +k, \pm l$
scan width	$\Delta\theta = 1.00 + 0.35 \tan\theta$	$\Delta\theta = 0.65 + 0.35 \tan\theta$	$\Delta\omega = 1.00 + 0.35 \tan\theta$
scan speed (θ, deg/m)	5.50	5.50	8.24 (ω, deg/min)
vert aperture (mm)	4.0	3.0	6.0
horiz aperture (mm)	$2.2 + 1.0 \tan\theta$	$2.0 + 1.0 \tan\theta$	$2.5 + 1.0 \tan\theta$
no. rflcns collected	1666	5019	5705
no. unique rflns	1498	4503	5673
no. obs rflcns ($F^2 > 3\sigma F^2$)	1425	2960	4519
I_{min}/I_{max}	0.56	0.86	0.76
no. parameters refined	117	385	316
$F(F)$ (%)	3.1	3.02	3.11
$R_w(F)$ (%)	3.9	2.90	3.02
R_{all} (%)	3.3	6.6	4.98
goodness of fit	1.86	1.13	1.019
p-factor	0.03	0.025	0.03

Table 3. Selected Intramolecular Distances (Å) for Complexes **1**, **2**, and **3a**

compd	atom 1	atom 2	distance
1	Ir	Zr	2.598(2)
	Ir	N	1.887(13)
	Zr	N	2.084(13)
	Ir	Cp3[a]	1.885
	Zr	Cp1	2.248
	Zr	Cp2	2.241
	N	C21	1.457(22)
2	Ir	N1	1.896(6)
	Ir	H1	1.58(6)
	Ir	Cp1	1.856
	Ir	Zr	2.977(1)
	H1	H2	1.75(9)
	Zr	N1	2.175(6)
	Zr	N2	2.220(7)
	Zr	H1	2.03(6)
	Zr	Cp2	2.270
	Zr	Cp3	2.275
	N1	C21	1.489(9)
	N1	H2	0.74(7)
	N2	C25	1.378(10)
3	Ir	Zr	3.020(1)
	Ir	N	1.889(6)
	Ir	H(B)	1.87
	Ir	Cp3	1.857
	Zr	O	2.083(5)
	Zr	N	2.149(6)
	Zr	H(B)	1.82
	Zr	Cp1	2.297
	Zr	Cp2	2.274
	N	C21	1.491(10)
	O	C25	1.330(9)

[a] In this and subsequent tables, distance and angles to Cp and Cp* refer to centroids. The lower Cp and Cp* ligand indices refer to the ligands with the lower atom indices in the figures.

(1)(μ-N-*t*-Bu)Ir(2)Cp*(PMePh$_2$) (Ir(1)–N = 1.81(1) Å).[42] Imido complex **1** was found to be remarkably stable to heat, undergoing no change at temperatures up to 130 °C.

Addition of Polar Organic Reagents to Complex 1. Addition of Amines and Ammonia. Although both iridium and zirconium formally have a 16-electron configuration, the addition of PMe$_3$ and *p*-(dimethylamino)pyridine to imido complex **1** resulted in no reaction at 45 °C. However, the addition of *p*-toluidine to the imido complex **1** at 25 °C resulted in an immediate reaction to form the N–H addition product Cp$_2$Zr(NHAr)(μ-N-*t*-Bu)(μ-H)IrCp* (**2**, Scheme 1). Red crystals of complex **2** were isolated in 60% yield from a mixture of toluene and pentane at −30 °C. Complex **2** was found to be thermally sensitive, decomposing over a 24-h period at 25 °C. Crystals of **2** suitable for X-ray diffraction were grown by slow cooling of a toluene solution to −30 °C. Complex **2** cocrystallized with 1 equiv of toluene. An ORTEP drawing is shown in Figure 2. Crystal parameters are given in Table 1, data collection parameters in Table 2, selected bond lengths in Table 3, and selected bond angles in Table 5. Both the hydride and the amide hydrogen were located and found to be outside of bonding distance to each other. The Ir–Zr distance of 2.977(1) Å is 0.38 Å longer than in the imido complex **1**, and the Ir–N–Zr angle has increased to 93.7(3)°, indicating a lack of bonding interaction between iridium and zirconium.

The *p*-toluidine addition product **2** is fluxional at 25 °C by ^{1}H NMR spectroscopy; neither the amide hydrogen nor the hydride was observed at this temperature. At −40 °C in toluene-d_8 the amide hydrogen was observed at +4.72 ppm and the hydride at −5.47 ppm. They were found to exchange with each other at −51 °C by a spin saturation transfer experiment. We believe the exchange is due to reversible N–H reductive elimination and oxidative addition. An N–H stretch was observed in the IR spectrum at 3366 cm^{-1} (Nujol), and a very weak hydride stretch was observed at 2096 cm^{-1} (Nujol). The formation of **2** was found to take place immediately at −80 °C by ^{1}H NMR spectroscopy.

The addition of *tert*-butylamine, isopropylamine, and neopentylamine to imido complex **1** resulted in no reaction. This is presumably due to their lower acidity compared to *p*-toluidine rather than their increased steric bulk since *tert*-butyl alcohol reacts readily with **1**, as discussed below. The addition of

Table 4. Selected Intramolecular Angles (deg) for Complex **1**

atom 1	atom 2	atom 3	angle
Ir	N	Zr	81.6(5)
Ir	N	C21	133.2(11)
Zr	N	C21	145.2(11)
Zr	Ir	N	52.5(4)
Zr	Ir	Cp3	151.5
N	Ir	Cp3	156.0
Ir	Zr	Cp1	116.6
Ir	Zr	Cp2	114.1
N	Zr	Cp1	113.0
N	Zr	Cp2	112.7
Ir	Zr	N	45.9(4)
Cp1	Zr	Cp2	130.1

Scheme 1

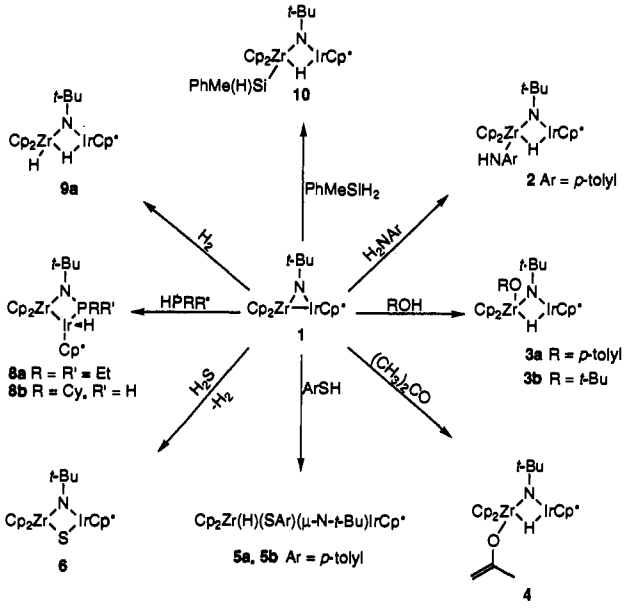

(41) Arney, D. J.; Bruck, M. A.; Huber, S. R.; Wigley, D. E. *Inorg. Chem.* **1992**, *31*, 3749.
(42) Dobbs, D. A.; Bergman, R. G. *J. Am. Chem. Soc.* **1993**, *115*, 3836.

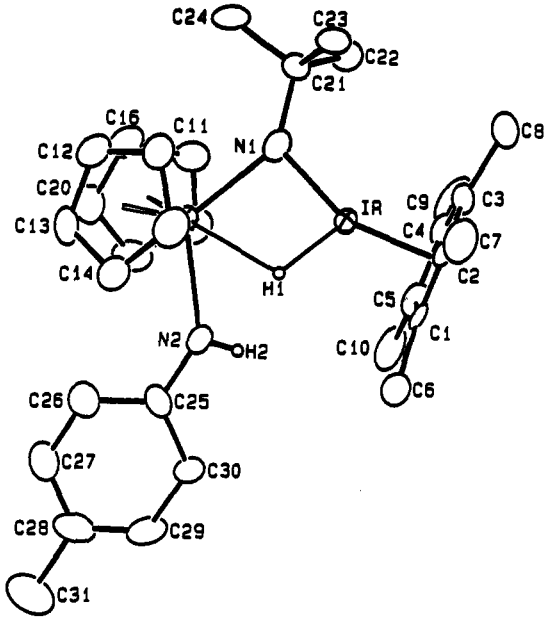

Figure 2. ORTEP diagram of $Cp_2Zr(NHAr)(\mu\text{-}H)(\mu\text{-}N\text{-}t\text{-}Bu)IrCp^*$ (**2**). Most hydrogen atoms are omitted for clarity.

Table 5. Selected Intramolecular Angles (deg) for Complex **2**

atom 1	atom 2	atom 3	angle
Ir	N1	Zr	93.7(3)
Ir	N1	C21	124.1(5)
Zr	N1	C21	142.0(5)
Ir	H1	Zr	110.4(32)
N1	Ir	H1	85.2(22)
Cp1	Ir	N1	153.6
Cp1	Ir	H1	121.2
N1	Zr	N2	122.6(2)
N1	Zr	H1	68.3(17)
H1	Zr	N2	56.0(17)
Cp2	Zr	N1	103.9
Cp3	Zr	N1	103.0
Cp2	Zr	N2	102.1
Cp3	Zr	N2	100.2
Cp2	Zr	H1	104.4
Cp3	Zr	H1	127.8
Zr	N2	C25	139.5(5)
Zr	N2	H2	112.8(63)
C25	N2	H2	107.2(64)

diphenylamine and 2,6-dimethylaniline to imido complex **1** also yielded no reaction, probably for steric reasons. The addition of (diphenylmethyl)amine or dimethylamine to **1** resulted in no reaction, while the addition of methylamine and ammonia resulted in decomposition at 25 °C.

Addition of Alcohols and Water. The addition of *p*-cresol to the imido complex **1** resulted in the immediate formation of the O–H addition product $Cp_2Zr(OAr)(\mu\text{-}N\text{-}t\text{-}Bu)(\mu\text{-}H)IrCp^*$ (**3a**, Scheme 1). Complex **3a** was isolated in 56% yield by slow cooling of a diethyl ether solution to –30 °C. Crystals suitable for an X-ray diffraction study were grown by cooling a solution of **3a** in a 3:1 ratio of diethyl ether and hexamethyldisiloxane from reflux to 25 °C. An ORTEP drawing is shown in Figure 3, crystal parameters are given in Table 1, data collection parameters in Table 2, selected bond lengths in Table 3, and selected bond angles in Table 6. The main difference between this structure and that of the *p*-toluidine addition product **2** is the arrangement of the ligands around zirconium. In the *p*-cresol addition product **3a** the bridging imide ligand occupies the central position in the equatorial wedge of zirconium, while in the *p*-toluidine addition product the hydride occupies the central position. A hydride resonance was observed in the ^1H NMR spectrum at –7.24 ppm in benzene-d_6, and a hydride stretch was observed in the IR spectrum at 1975 cm^{-1} (Nujol). This compound was not found

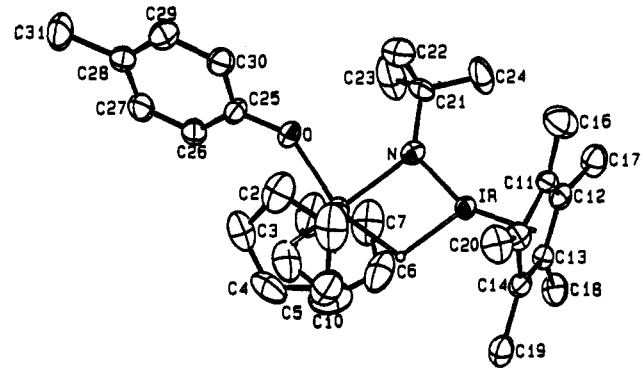

Figure 3. ORTEP diagram of $Cp_2Zr(OAr)(\mu\text{-}H)(\mu\text{-}N\text{-}t\text{-}Bu)IrCp^*$ (**3a**). Most hydrogen atoms are omitted for clarity.

Table 6. Selected Intramolecular Angles (deg) for Complex **3a**

atom 1	atom 2	atom 3	angle
Ir	N	Zr	96.6(3)
Ir	N	C21	128.1(5)
Zr	N	C21	134.9(5)
Ir	H(B)	Zr	109.9
Zr	Ir	N	44.98(19)
Zr	Ir	H(B)	34.5
Zr	Ir	Cp3	153.2
N	Ir	H(B)	78.9
N	Ir	Cp3	127.7
Ir	Zr	O	123.47(14)
Ir	Zr	N	38.41(15)
Ir	Zr	H(B)	35.5
Ir	Zr	Cp1	103.5
Ir	Zr	Cp2	105.6
O	Zr	N	86.31(20)
O	Zr	H(B)	158.8
O	Zr	Cp1	98.3
O	Zr	Cp2	103.5
N	Zr	H(B)	73.4
N	Zr	Cp1	122.7
N	Zr	Cp2	109.3
H(B)	Zr	Cp1	88.2
H(B)	Zr	Cp2	89.1
Cp1	Zr	Cp2	124.5
Zr	O	C25	144.4

to be fluxional by ^1H NMR spectroscopy at room temperature and was stable for prolonged periods at 25 °C.

The addition of *p*-cresol to imido complex **1** was also carried out and monitored by ^1H NMR spectroscopy at low temperature. An immediate reaction was observed at –80 °C to form a species which then proceeded to **3a** at –40 °C. The intermediate had a ^1H NMR spectrum similar to that of the final product **3a**, including a hydride resonance at –4.99 ppm. A NOESY experiment performed at –70 °C provided evidence that the initial product is another isomer of **3a**, which has its hydride and cresolate ligands cis rather than trans to each other, as should result from a concerted addition of *p*-cresol to **1** (eq 2). An NOE cross peak

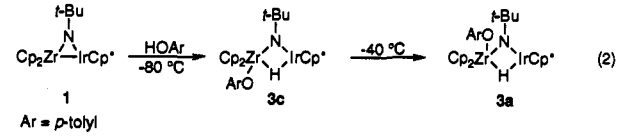

was observed in the NOESY spectrum of the intermediate between the hydride and the ortho protons on the cresolate ligand. No cross peak was observed between the ortho protons on the cresolate ligand and the imido ligand. A NOESY spectrum of **3a** revealed a cross peak between the imido ligand and the ortho protons of the cresolate ligand and not between the hydride and the ortho protons. The isomerization could take place by dissociation of the bridging hydride ligand from zirconium, rotation around the

Zr–N bond, and then reassociation of the bridging hydride ligand, but we do not know whether it is intra- or intermolecular.

In contrast to *tert*-butylamine, *tert*-butyl alcohol reacted immediately at 25 °C with imido complex **1** to form the O–H addition product $Cp_2Zr(O\text{-}t\text{-}Bu)(\mu\text{-}N\text{-}t\text{-}Bu)(\mu\text{-}H)IrCp^*$ (**3b**, Scheme 1). Complex **3b** was isolated as red crystals from diethyl ether in 74% yield. A hydride resonance was observed in the ^1H NMR spectrum at −6.03 ppm in benzene-d_6, and a hydride stretch was observed in the IR spectrum at 2024 cm^{-1} (Nujol). Due to its spectroscopic similarity to the *p*-cresol addition product **3a**, we have assigned **3b** a similar structure, as shown in Scheme 1. However, we are not certain if the *tert*-butoxide ligand is cis to the imido ligand as drawn or cis to the hydride ligand as in the *p*-toluamide complex **2**. The addition of water to imido complex **1** in THF-d_8 resulted in decomposition at 25 °C.

Addition of Acetone. The addition of acetone to the imido complex **1** reacted over several hours to form the enolate complex $Cp_2Zr(OC(CH_2)CH_3)(\mu\text{-}N\text{-}t\text{-}Bu)(\mu\text{-}H)IrCp^*$ (**4**, Scheme 1). Resonances for the methylene protons were observed at 4.14 and 4.07 ppm in benzene-d_6, which are values typical for zirconocene oxygen-bonded enolates.[43–47] A small coupling constant (^2J = 1 Hz) was observed in only one of the resonances. A hydride resonance was observed at −7.29 ppm, which is similar to that of the *p*-cresol (**3a**), *p*-toluidine (**2**), and *tert*-butyl alcohol (**3b**) addition products. A metal hydride stretch was observed in the IR spectrum at 1974 cm^{-1} in Nujol, and a C=C stretch was observed at 1605 cm^{-1}. The terminal vinylic carbon appears at 83.7 ppm in the ^{13}C NMR spectrum. These data lead us to postulate that the structure of **4** is that shown in Scheme 1, with a zirconium O-bonded enolate and a hydride bridging the two metal centers.

Addition of *p*-Thiocresol and H_2S. The addition of *p*-thiocresol to imido complex **1** resulted in the formation of a 90:10 mixture of two products ($Cp_2Zr(SAr)(H)(\mu\text{-}N\text{-}t\text{-}Bu)IrCp^*$, **5a**, **5b**). These compounds were determined to be in equilibrium by a two-dimensional exchange experiment (EXSY) at 45 °C by NMR spectroscopy. The major product is spectroscopically similar to the *p*-toluidine (**2**), *p*-cresol (**3a**), *tert*-butyl alcohol (**3b**), and acetone (**4**) addition products and therefore presumably structurally similar to these complexes. A hydride resonance for the major product was observed at −3.93 ppm in the ^1H NMR spectrum. A hydride stretch was observed in the IR spectrum at 1974 cm^{-1}. The minor product has diastereotopic Cp resonances, implying a chiral center at iridium; however, we are not certain of its structure.

In contrast to H_3N and H_2O, H_2S reacted with imido complex **1** at 25 °C to give the bridging sulfido complex **6** ($Cp_2Zr(\mu\text{-}N\text{-}t\text{-}Bu)(\mu\text{-}S)IrCp^*$) in 44% yield by ^1H NMR spectroscopy and dihydrogen. Sulfido complex **6** has previously been prepared by the addition of $SPMe_3$ to the imido complex **1**.[23] One possible mechanism for the reaction involves initial S–H oxidative addition, as occurs with alcohols and amines, followed by elimination of H_2 (eq 3). When the reaction was monitored at low temperature

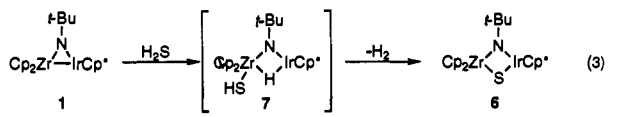

(3)

by ^1H NMR spectroscopy, several unidentified intermediates were observed. The addition of 3 atm of dihydrogen to sulfido complex **6** resulted in no reaction rather than the formation of the possible hydridothiolate intermediate **7**.

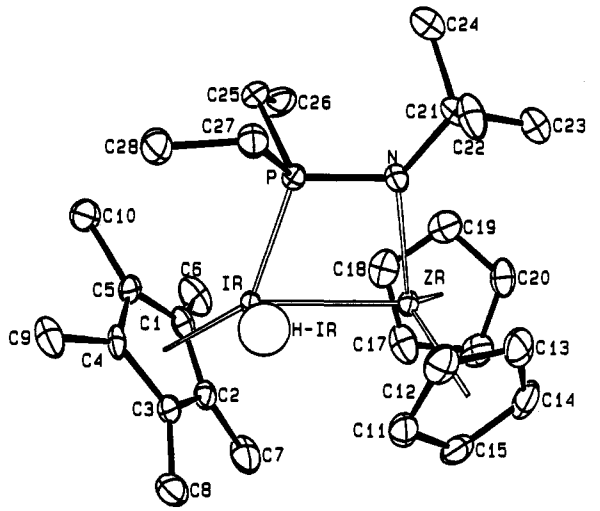

Figure 4. ORTEP diagram of $Cp_2Zr(\mu\text{-}N(t\text{-}Bu)PEt_2)Ir(H)(Cp^*)$ (**8a**). Most hydrogen atoms are omitted for clarity.

Table 7. Crystal Parameters for Complexes **8a**, **9a**, and **11**

	8a[a]	**9a**[b,c]	**11**[d]
empirical formula	$C_{28}H_{45}IrNPZr$	$C_{31}H_{44}IrNZr$	$C_{24}H_{39}F_3IrNO_4SZr$
formula wt (amu)	710.1	714.1	778.1
crystal size	0.17 × 0.21 × 0.35	0.23 × 0.30 × 0.37	0.30 × 0.30 × 0.55
space group	$P2_1/n$	$Pnma$	$P2_1/n$
a (Å)	9.5153(14)	12.214(2)	9.2222(11)
b (Å)	19.3536(20)	12.806(1)	16.571(2)
c (Å)	15.0471(20)	18.353(3)	20.046(2)
β (deg)	104.651(20)	90.0	99.881(9)
V (Å^3)	2680.9(12)	2870.4(11)	3018.0(12)
Z	4	4	4
d_{calc} (g cm^{-3})	1.76	1.65	1.71
μ_{calc} (cm^{-1})	54.0	49.9	48.4

[a] Unit cell parameters and their esd's were derived by a least-squares fit to the setting angles of the unresolved Mo Kα components, 24 reflections with 2θ between 28 and 32°. [b] Unit cell parameters and their esd's were derived by a least-squares fit to the setting angles of the unresolved Mo Kα components, 24 reflections with 2θ equal to 30°. [c] Complex **9a** cocrystallized with 1 equiv of toluene. [d] Unit cell parameters and their esd's were derived by a least-squares fit to the setting angles of the unresolved Mo Kα components, 24 reflections with 2θ between 28 and 34°.

Addition of Phosphines. Addition of diethylphosphine to imido complex **1** resulted in the insertion of diethylphosphide (PEt_2) into the Ir–N bond to form complex $Cp_2Zr(\mu\text{-}N(t\text{-}Bu)PEt_2)Ir(H)Cp^*$ (**8a**, Scheme 1). Complex **8a** was isolated in 63% yield as dark red crystals by cooling a solution of diethyl ether to −30 °C. Crystals suitable for X-ray diffraction were grown in this manner, and the ORTEP drawing is shown in Figure 4. Crystal parameters are given in Table 7, data collection parameters in Table 8, selected bond distances in Table 9, and selected bond angles in Table 10. The P–N bond length (1.666(3) Å) is indicative of a single bond,[48] and the Ir–Zr bond length (2.642(1) Å) is comparable to that of the starting material **1**. Complex **8a** was examined by variable temperature ^1H NMR spectroscopy. At 50 °C the cyclopentadienyl resonances appeared as a single line, while at −40 °C they were observed to be diastereotopic due to the chiral center at iridium. The hydride resonance, observed in the ^1H NMR spectrum at −14.16 ppm with $^2J_{PH}$ = 29 Hz, did not vary between −80 and +50 °C. When the reaction was monitored at low temperature by ^1H NMR spectroscopy, several intermediates were observed, and these were converted to complex **8a** at 10 °C. The addition of 10 equiv of cyclohexylphosphine

(43) Veya, P.; Floriani, C.; Chiesi-Villa, A.; Guastini, C. *Organometallics* **1991**, *10*, 2991.
(44) Manriquez, J. M.; McAlister, D. R.; Sanner, R. D.; Bercaw, J. E. *J. Am. Chem. Soc.* **1978**, *100*, 2716.
(45) Moore, E. J.; Straus, D. A.; Armantrout, J.; Santarsiero, B. D.; Grubbs, R. H.; Bercaw, J. E. *J. Am. Chem. Soc.* **1983**, *105*, 2068.
(46) Erker, G.; Dorf, U.; Lecht, R.; Ashby, M. T.; Aulbach, M.; Schlund, R.; Krüger, C.; Mynott, R. *Organometallics* **1989**, 8.
(47) Curtis, M. D.; Thanedar, S.; Butler, W. M. *Organometallics* **1984**, *3*, 1855.
(48) Dehnicke, K.; Strähle, J. *Polyhedron* **1989**, *8*, 707.

Table 8. Data Collection Parameters for Complexes **8a**, **9a**, and **11**

	8a	9a	11
temp (°C)	−110	−106	−99
rflcns measd	$+h, +k, \pm l$	$+h, \pm k, +l$	$+h, +k, \pm l$
scan width	$\Delta\theta = 0.85 + 0.35 \tan\theta$	$\Delta\theta = 0.75 + 0.35 \tan\theta$	$\Delta\theta = 0.75 + 0.35 \tan\theta$
scan speed (θ, deg/m)	5.49	5.49	5.49
vert aperture (mm)	4.0	3.0	3.0
horiz aperture (mm)	$2.2 + 1.0 \tan\theta$	$2.0 + 1.0 \tan\theta$	$2.0 + 1.0 \tan\theta$
no. rflcns collected	4875	5641	5504
no. unique rflcns	4711	3429	5294
no. obs rflcns ($F^2 > 3\sigma F^2$)	3958	2607	3870
I_{max}/I_{min}	0.76	0.56	0.71
no. parameters refined	470	264	316
$R(F)$ (%)	1.97	2.50	2.86
$R_w(F)$ (%)	2.25	2.76	3.15
R_{all} (%)	2.93	4.28	5.08
goodness of fit	1.078	1.014	1.244
p-factor	0.03	0.03	0.03

Table 9. Selected Intramolecular Distances (Å) for Complexes **8a**, **9a**, and **11**

compd	atom 1	atom 2	distance
8a	Ir	Zr	2.642(1)
	Ir	P	2.235(1)
	Ir	H-Ir	1.39(6)[a]
	Ir	Cp1	1.985
	Zr	N	2.164(3)
	P	N	1.666(3)
	Zr	Cp3	2.289
	Zr	Cp2	2.307
	N	C21	1.499
	P	C25	1.838(4)
	P	C27	1.838(4)
9a	Ir	Zr	2.947(1)
	Ir	N	1.887(5)
	Ir	H(B)	1.50(6)
	Zr	N	2.152(5)
	Zr	H(B)	1.90(6)
	Zr	H(T)	1.84(8)
	N	C7	1.499(8)
	Ir	Cp1	1.854(1)
	Zr	Cp2	2.241(1)
11	Ir	Zr	2.965(1)
	Ir	N	1.918(5)
	Ir	H(B)	1.28(8)
	Zr	O1	2.186(4)
	Zr	O4	1.917(4)
	Zr	N	2.085(5)
	Zr	H(B)	2.12(7)
	N	C16	1.489(7)
	Zr	Cp2	2.236
	Ir	Cp1	1.830

[a] Note that the Ir–H distance is shorter than the ca. 1.6 Å that would normally be expected. It appears to be located in a reasonable position, and so we have included it in the ORTEP diagram.

or 5 equiv of trimethylphosphine to complex **8a** did not result in displacement of the phosphineamide ligand from iridium. It is not surprising that the chelating phosphine is preferred over the nonchelating phosphine.

Cyclohexylphosphine was also found to react with imido complex **1** to give an analogous compound $Cp_2Zr(\mu\text{-}N(t\text{-}Bu)\text{-}PHCy)Ir(H)Cp^*$ (**8b**, Scheme 1). A hydride resonance was observed in the ^1H NMR spectrum at −14.67 ppm with a coupling constant of $^2J_{PH}$ = 29.9 Hz, and the P–*H* was observed at 5.14 ppm, $^1J_{PH}$ = 349 Hz. The cyclohexyl reaction product **8b** is not fluxional at room temperature by ^1H NMR spectroscopy. The cyclopentadienyl ligands are diastereotopic from −80 to +50 °C, and only one of the two possible diastereomers was observed. A ^{31}P decoupled NOESY experiment revealed an NOE cross peak between the cyclohexyl protons and the hydride ligand but not between the P–*H* and the hydride ligand. A cross peak was also observed between one of the Cp ligands and both the hydride and cyclohexyl ligands. No cross peaks between the hydride and cyclohexyl ligands and the other Cp ligand were observed. This suggests that the cyclohexyl and hydride ligands are cis to each other in the diastereomer observed. The addition of phenylphosphine to imido complex **1** resulted in decomposition at 25 °C.

Table 10. Selected Intramolecular Angles (deg) for Complex **8a**

atom 1	atom 2	atom 3	angle
Zr	Ir	P	71.62(3)
Zr	Ir	H-Ir	80.8(23)
Zr	Ir	Cp1	141.91
P	Ir	H-Ir	84.9(23)
P	Ir	Cp1	140.25
H-Ir	Ir	Cp1	115.2
Ir	Zr	N	82.71
Ir	Zr	Cp2	112.07
Ir	Zr	Cp3	111.27
N	Zr	Cp2	112.57
N	Zr	Cp3	109.66
Cp2	Zr	Cp3	121.84
Ir	P	N	109.13(12)
Zr	N	P	96.31(15)
Zr	N	C21	134.6(3)
P	N	C21	128.6(3)

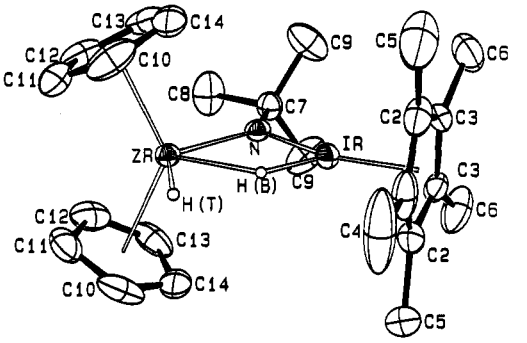

Figure 5. ORTEP diagram of $Cp_2Zr(H)(\mu\text{-}H)(\mu\text{-}N\text{-}t\text{-}Bu)IrCp^*$ (**9a**). Most hydrogen atoms are omitted for clarity.

Addition of Methyl Iodide, Methyl Triflate, and Trimethylsilyl Chloride. We were interested in observing the oxidative addition of polar X–Y bonds to the metal–metal bond of the imido complex **1**. Methyl iodide is the classic oxidative addition reagent, but its addition to **1** resulted in no reaction at 25 °C and decomposition at 45 °C. Treatment of **1** with methyl triflate resulted in decomposition at 25 °C. The addition of trimethylsilyl chloride to **1** also resulted in no reaction at 25 °C and decomposition at 45 °C.

Addition of Nonpolar Reagents to Complex 1. Addition of H_2. Addition of 650 Torr of H_2 to a solution of imido complex **1** in diethyl ether at 25 °C resulted in the clean formation of the dihydride complex $Cp_2Zr(H)(\mu\text{-}N\text{-}t\text{-}Bu)(\mu\text{-}H)IrCp^*$ (**9a**, Scheme 1). Complex **9a** was found to be thermally unstable, decomposing at 25 °C within one day. The dihydride **9a** was crystallized by reducing the volume of diethyl ether and cooling to −30 °C. Single crystals were grown in this manner and examined by X-ray crystallographic techniques. An ORTEP drawing is shown in Figure 5. Crystal parameters are given in Table 7, data collection parameters in Table 8, selected bond lengths in Table 9, and selected bond angles in Table 11. The ^1H NMR spectrum contains separate resonances for each hydride at −0.71 and −1.95 ppm, $^2J_{HH}$ = 6 Hz. There should be two metal hydride stretches in the IR spectrum; however, only one very weak absorption was observed in the hydride region at 1986 cm^{-1}. The addition of dihydrogen was found to be reversible. Dihydrogen was removed by applying an active vacuum to a toluene solution of dihydride **9a**, resulting in the regeneration of imido complex **1**. Heating a benzene-d_6 solution of the dihydride **9a** under 1 atm of H_2

Table 11. Selected Intramolecular Angles (deg) for Complex **9a**

atom 1	atom 2	atom 3	angle
Ir	N	Zr	93.48(20)
Ir	N	C7	127.3(4)
Zr	N	C7	139.2(4)
Ir	H(B)	Zr	119.8(37)
Zr	Ir	N	46.79(14)
Zr	Ir	H(B)	34.0(24)
Zr	Ir	Cp1	155.33(15)
N	Ir	H(B)	80.8(24)
N	Ir	Cp1	155.33(15)
H(B)	Ir	Cp1	123.8(24)
Ir	Zr	N	39.73(13)
Ir	Zr	H(B)	26.2(18)
Ir	Zr	H(T)	82.6(24)
Ir	Zr	Cp2	115.08(1)
N	Zr	H(B)	65.9(18)
N	Zr	H(T)	122.3(25)
N	Zr	Cp2	107.88(4)
H(B)	Zr	H(T)	56.4(29)
H(B)	Zr	Cp2	113.2(3)
H(T)	Zr	Cp2	94.8(10)

resulted in broadening of the hydride resonances in the ^{1}H NMR spectrum into the base line at 55 °C. Coalescence could not be observed upon further heating due to sample decomposition.

Addition of D_2 to complex **1** resulted in the formation of the analogous dideuteride complex $Cp_2Zr(D)(\mu$-N-*t*-Bu$)(\mu$-D)IrCp* (**9b**). Deuterium was found to be incorporated into the Cp rings over a period of 3 h by ^{2}H NMR spectroscopy. Small hydride peaks were observed in the ^{1}H NMR spectrum of **9b** due to incorporation of hydrogen into the hydride position from the Cp rings. Due to the weak Ir–H stretch, an Ir–D stretch could not be assigned in the IR spectrum. The addition of a 50/50 mixture of D_2 and H_2 to the imido complex **1** resulted in the formation of H–D by ^{1}H NMR spectroscopy over a period of 4 h (eq 4).

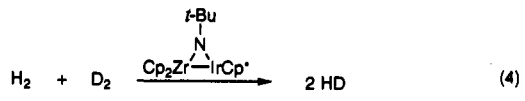

(4)

The addition of the dideuteride **9b** to the dihydride **9a** resulted in exchange of label to give the hydridodeuterides **9c** and **9d**, as shown by ^{1}H NMR spectroscopy (eq 5).

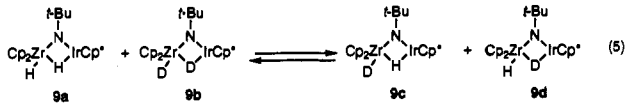

(5)

Addition of Silanes. Addition of excess methylphenylsilane to the imido complex **1** resulted in rapid reaction at room temperature to give a Si–H addition product that we propose to be Cp_2Zr-(SiH(Me)(Ph))$(\mu$-N-*t*-Bu$)(\mu$-H)IrCp* (**10**, Scheme 1). This reaction was found to be reversible, in analogy to the H_2 reaction. Complex **10** was unstable in solution in the absence of an excess of silane and was not isolated. The crude reaction mixture was characterized by ^{1}H NMR, ^{13}C NMR, and IR spectroscopies. A hydride resonance similar to that of the dihydride **9a** was observed in the ^{1}H NMR spectrum at –3.71 ppm. The Cp ligands were observed to be diastereotopic in the ^{1}H and ^{13}C{^{1}H} spectra. An absorption at 2006 cm^{-1} in the IR spectrum could be assigned to either a Si–H or a metal hydride stretch.

The addition of phenylsilane and diphenylsilane resulted in the formation of similar products by ^{1}H NMR spectroscopy, but their instability prevented isolation.

Reactions of the *p*-Cresol, *p*-Toluidine, and *tert*-Butyl Alcohol Addition Products. Addition of Methyl Triflate to the *tert*-Butyl Alcohol Addition Product 3b. Somewhat unexpectedly, addition of methyl triflate to the *tert*-butoxide complex **3b** yielded methylcyclopentadiene and a new material that exhibited res-

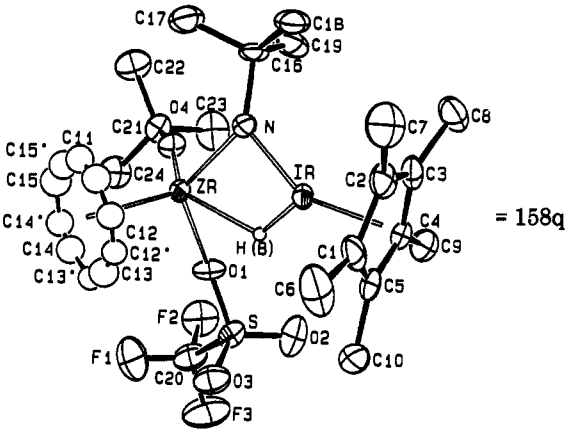

= 158q

Figure 6. ORTEP diagram of CpZr(O-*t*-Bu)(OTf)$(\mu$-H)$(\mu$-N-*t*-Bu)-IrCp* (**11**). Most hydrogen atoms are omitted for clarity.

Table 12. Selected Intramolecular Angles (deg) for Complex **11**

atom 1	atom 2	atom 3	angle
Ir	N	Zr	95.47(20)
Ir	N	C16	130.9(4)
Zr	N	C16	132.6(4)
Ir	H(B)	Zr	119.2(45)
Zr	Ir	Cp1	163.65
N	Ir	Cp1	151.04
H(B)	Ir	Cp1	125.4
N	Ir	H(B)	83.1(32)
Ir	Zr	O1	93.00(12)
Ir	Zr	O4	125.92(12)
Ir	Zr	Cp2	114.76
Cp2	Zr	O1	108.69
Cp2	Zr	O4	116.29
Cp2	Zr	N	117.11
Cp2	Zr	H(B)	108.1
N	Zr	H(B)	62.2(20)
H(B)	Zr	O1	75.0(20)
O1	Zr	O4	86.93(17)
O4	Zr	N	99.07(18)
Zr	O1	S	147.4(3)
Zr	O4	C21	165.0(4)

onances in the ^{1}H NMR spectrum for single Cp, *tert*-butoxy, and Cp* groups. Methylcyclopentadiene was identified by GCMS.[49] The organometallic product was purified in 62% yield by crystallization from a mixture of diethyl ether and hexamethyldisiloxane at 25 °C. Crystals grown under these conditions were characterized by an X-ray diffraction study, which demonstrated that the material is complex **11** (CpZr(O-*t*-Bu)(OTf)-$(\mu$-H)$(\mu$-N-*t*-Bu)IrCp*), shown in eq 6.

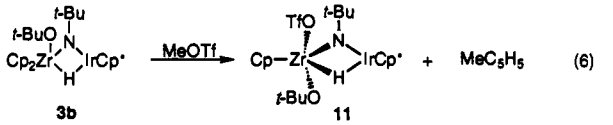

(6)

The ORTEP drawing in Figure 6 shows that the triflate is covalently bonded to zirconium in the solid state. Crystal parameters are given in Table 7, data collection parameters in Table 8, selected bond distances in Table 9, and selected bond angles in Table 12. Absorbances were observed in the IR spectrum at 1340 and 1240 cm^{-1} in C_6D_6 and 1337 and 1234 cm^{-1} in a Nujol mull. Typically, a strong resonance at 1270 cm^{-1} indicates an ionic triflate anion, and a resonance at 1370 cm^{-1} indicates a covalently bonded triflate.[50] The solution- and solid-state IR values we obtained are not definitive for the presence of either covalently or ionically bonded triflates. A hydride resonance

(49) The yield of methylcyclopentadiene was determined to be 18% by GC. We did not identify the products from the remaining cyclopentadiene ligand.

(50) Lawrance, G. A. *Chem. Rev.* **1986**, *86*, 17.

Scheme 2

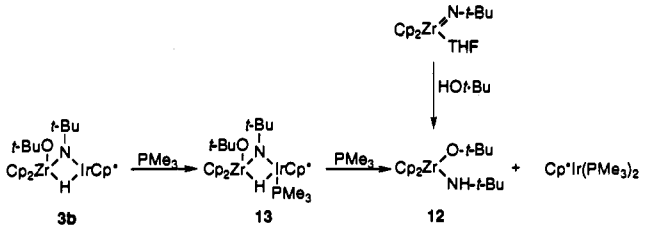

was observed in the ^1H NMR spectrum in C_6D_6 at −5.33 ppm which is similar to the chemical shifts of the other bridging hydrides we have observed. A hydride stretch was observed in the IR spectrum at 1950 cm^{-1} (Nujol).

The addition of MeLi to the triflate complex **11** resulted in decomposition at 25 °C. The addition of MeMgCl resulted in no reaction at 25 °C. Prolonged heating of a solution of 1/3 equiv of Me_3Al and the triflate complex **11** resulted in no reaction at 70 °C.

Addition of Phosphines to the N–H and O–H Addition Products 2, 3a, and 3b. The addition of 2 equiv of PMe_3 to the *tert*-butoxide complex **3b** resulted in the elimination of $Cp_2Zr(O$-*t*-$Bu)(NH$-*t*-$Bu)$ (**12**) and the formation of $Cp^*Ir(PMe_3)_2$ at 25 °C over 2 days (Scheme 2). These products could not be separated from each other. The zirconium complex was synthesized independently by the addition of *tert*-butyl alcohol to $Cp_2Zr(N$-*t*-$Bu)(THF)$ in benzene at 25 °C (Scheme 2). $Cp^*Ir(PMe_3)_2$ was previously synthesized by workers in our laboratory.[51] When the reaction was monitored by ^1H NMR spectroscopy, an intermediate was observed with two resonances apparently due to diastereotopic Cp ligands and a hydride resonance at −16.64 ppm, $^2J_{PH}$ = 26.2 Hz. We propose that this compound is the PMe_3 adduct **13** (Scheme 2).

The addition of triphenylphosphine to the *tert*-butoxide complex yielded no reaction. The addition of PMe_3 or PPh_3 to the *p*-cresolate (**3a**) or *p*-toluamide (**2**) complex resulted in no reaction.

Addition of Strong Bases and Trityl Cation to 2 and 3a. We wished to abstract either a proton or hydride from the *p*-toluidine (**2**) or *p*-cresol (**3a**) addition products. However, the addition of $LiN(SiMe_3)_2$ or MeLi to the toluamide complex **2** resulted in the formation of imido complex **1** along with some decomposition at 25 °C. The addition of MeLi to the *tert*-butoxide complex **3a** also resulted in the formation of imido complex **1**. The addition of trityl cation to the toluamide complex **2** resulted in decomposition at 25 °C.

Attempted Catalytic Hydrogenation Reactions. The addition of dihydrogen and ethylene to the imido complex **1** (5 mol %) in C_6D_6 at 25 °C resulted in hydrogenation of ethylene to ethane at a rate of 10 turnovers per hour. The organometallic species in solution during the catalytic reaction was observed to be the dihydride complex **9a** by ^1H NMR spectroscopy. In the absence of H_2 neither the imido complex **1** nor the dihydride **9a** reacted with ethylene. The addition of 5 equiv of PMe_3 to a solution of imido complex **1** (5 mol %), dihydrogen, and ethylene resulted in complete inhibition of hydrogenation without the formation of a PMe_3 adduct with dihydride **9a**. This result implies that the reaction is catalyzed by a decomposition product or other impurity present in small quantities in the reaction mixture rather than **9a**. The catalyst appears to be homogeneous since addition of Hg to the hydrogenation reaction mixture did not have an effect on the rate of reaction.[52] Dihydride **9a** is thermally sensitive, and so progressive decomposition was seen in all of the hydrogenation reactions.

The addition of 1-butene and H_2 to imido complex **1** (10 mol %) resulted in the isomerization of 1-butene to *cis*- and *trans*-2-butene and also in the formation of butane. In the absence of H_2 neither imido complex **1** nor dihydride **9a** catalyzed the isomerization of 1-butene to *cis*- and *trans*-2-butene. Propylene, *cis*- and *trans*-2-butene, 1-phenyl-1-propyne, 3-hexyne, and *N*-phenylbenzaldimine were also observed to be hydrogenated upon addition of H_2 and imido complex **1**.

The addition of H_2, silanes, and ethylene to imido complex **1** did not result in the hydrosilation of ethylene with phenylsilane, diphenylsilane, triphenylsilane, trimethylsilane, or methylphenylsilane. The addition of methylphenylsilane and 1-phenyl-1-propyne to **1** resulted only in decomposition at 45 °C. The addition of synthesis gas to imido complex **1** resulted in decomposition at 25 °C.

Discussion

The reaction that results in the synthesis of the early–late heterobimetallic bridging imido complex **1** can be thought of as a substitution of the butene ligand in $Cp_2Zr(CH_2{=}CHCH_2CH_3)$ with Cp^*IrN-*t*-Bu (eq 7),resulting in the coordination of

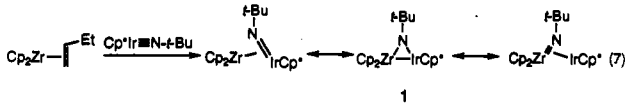

(7)

the iridium imide complex to Zr(II). In previously studied zirconocene alkene and alkyne complexes, back-bonding into the alkene and alkyne, to give metallacyclopropane or metallacyclopropene resonance structures, has been postulated.[53] The structure of imido complex **1** suggests that there is also a significant amount of back-bonding from zirconium to the iridium imide complex which leads to a quasi-symmetric three-membered ring. Both the Ir–N and Zr–N bond lengths are consistent with M–N single bonds. An additional resonance structure in which a zirconocene imide complex is coordinated to iridium can also be formulated, but once again the relatively symmetric structure of the complex argues against this interpretation. The bridging imido ligand in **1** is planar at nitrogen, implying donation of the nitrogen lone pair to the ring's orbital system.

Despite being formally coordinatively unsaturated at both metal centers, **1** does not react with donor ligands such as PMe_3 or *p*-(dimethylamino)pyridine. However, this property does make both metal centers available for reaction with organic substrates. We expected that ligands with "hard" heteroatoms (O and N) would add across the Zr–Ir bond, giving products in which the heteroatom was bonded to zirconium, while ligands with "soft" heteroatoms (S and P) would add across the Zr–Ir bond to give products in which the heteroatom was bonded to iridium.[54,55] Thus, we compared the reactivity of **1** with amines, alcohols, acetone, thiols, and phosphines. *p*-Toluidine, *p*-cresol, *tert*-butyl alcohol, and acetone reacted as expected to give a zirconium-bonded amide (**2**), aryloxide (**3a**), alkoxide (**3b**), and enolate (**4**), respectively (Scheme 1). The addition of *p*-thiocresol appeared to give a zirconium-bonded thiolate as its major product (**5a**), but this complex was in equilibrium with another product (**5b**). A proposed mechanism for the X–H additions, shown in eq 8, involves prior coordination of the heteroatom to zirconium followed by proton transfer to the iridium center. The prior coordination would be particularly important for *p*-toluidine and acetone to increase the acidity of the proton transferred. Phosphines gave

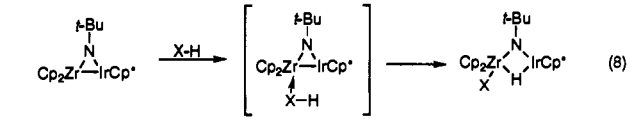

(8)

(51) McGhee, W. D.; Bergman, R. G. *J. Am. Chem. Soc.* **1988**, *110*, 4246.
(52) Whitesides, G. M.; Hackett, M.; Brainard, R. L.; Lavalleye, J.-P. P. M.; Sowinski, A. F.; Izumi, A. N.; Moore, S. S.; Brown, D. W.; Staudt, E. M. *Organometallics* **1985**, *4*, 1819.
(53) Buchwald, S. L.; Nielsen, R. B. *Chem. Rev.* **1988**, *88*, 1047.
(54) Pearson, R. G. *J. Am. Chem. Soc.* **1963**, *85*, 3533.
(55) Pearson, R. G. *J. Chem. Ed.* **1968**, *45*, 643.

an entirely different and unexpected reaction with **1**, adding across the Ir–N rather than the Zr–Ir linkage to form a product with an Ir–P bond. Thus, **1** reacted with organic reagents containing O and N to form Zr–O and Zr–N bonds and with phosphines to form an Ir–P bond.

The insertion of phosphide into the Ir–N bond to form the phosphine amide complexes **8a** and **8b** has little precedent. There are few compounds known containing phosphine amides bonded through both N and P to either one or two metal centers.[56–58] Monitoring the reaction of diethylphosphine with imido complex **1** by variable temperature ^{1}H NMR spectroscopy indicated that the reaction is complicated, involving several intermediates. The reaction could proceed by a P–H addition across the Zr–Ir bond, analogous to the other X–H addition reactions we have observed, followed by insertion of the phosphide moiety into the Ir–N bond. Alternatively, the reaction could take place entirely at the iridium center. The fluxional behavior we observe in the ^{1}H and ^{13}C{^{1}H} NMR spectra for the diethylphosphine product **8a** can be explained by reversible dissociation from iridium of the phosphine ligand, resulting in epimerization at iridium. The lack of fluxional behavior in the cyclohexylphosphine product is possibly due to the greater steric interaction of the cyclohexyl ligand with the Cp* than the P–H with the Cp*. The structure with the cyclohexyl ligand directed away from the Cp* is therefore preferred, and only one diastereomer is observed. The chemical shifts of the hydride ligands in both **8a** and **8b** are dramatically different from those of the complexes with bridging hydrides because the former are terminal hydrides bonded to 18-electron iridium centers. However, the hydride stretch in the IR spectrum is similar to those observed in complexes with bridging hydride ligands.

An interesting feature of the structurally characterized *p*-toluidine (**2**), *p*-cresol (**3a**), and dihydrogen (**9a**) addition products is the hydride bridging the two metal centers. The closely related complexes Cp*Ir(NHCH$_2$Ph)(H)(PPh$_3$) and Cp*Ir(NHPh)(H)(PPh$_3$) are not observed without the dative phosphine ligand.[59] Not only do the X–H addition products **2**, **3a**, and **9a** not require a dative ligand at the unsaturated 16-electron iridium center but the hydride is bridging to zirconium. The bridging hydride is also unusual since zirconocene bisamides and bisalkoxides are stable as 16-electron species.[60] There is no evidence of shortening of the bond between the imido ligand and iridium in the X-ray crystal structures, which might suggest an increase in π-bonding between iridium and the amide nitrogen. However, the Zr–N bond is longer in **2**, **3a**, and **9a** than in **1** by 0.06–0.09 Å. We propose that the stability of the 16-electron iridium center in these X–H addition products indicates that the early metal interacts with the late metal in these complexes despite the absence of full metal–metal bonds.

The *p*-cresol (**3a**) and *p*-toluidine (**2**) addition products differ in geometry at zirconium. In **3a** the dative hydride ligand is in the outside position of the equatorial wedge at zirconium, while in **2** it is in the central position. Because *p*-cresol and *p*-toluidine are similar in size, we believe that the difference in geometry is electronic in origin. The initial product formed in the *p*-cresol reaction at –80 °C appears to be **3c**, an intermediate in which the hydride and cresolate ligands are cis to each other, as observed in the *p*-toluamide complex **2**. This compound isomerizes to the isolated product **3a** at –40 °C. Similar isomerizations have been observed with acyl and thioacyl complexes of zirconium.[61–65] A thorough investigation of the addition of CO to Cp$_2$ZrMe$_2$ was carried out by Erker and co-workers.[61] They found that the acyl ligand with the carbonyl group outside the wedge was formed at –130 °C, and then at –123 °C an isomerization took place to form the acyl with the carbonyl inside the wedge (eq 9). A

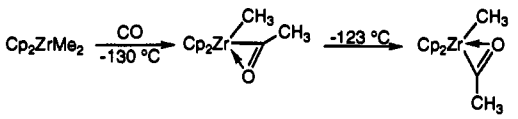

(9)

theoretical study suggested that the LUMO of Cp$_2$ZrMe$_2$ was directed primarily outside the wedge but better total overlap existed between the acyl ligand and d orbitals of zirconium inside the wedge, leading to the final thermodynamic product.[65] We do not have an explanation for why the *p*-toluidine addition product (**2**) should be more stable with the dative hydride ligand in the center of the wedge while the *p*-cresol addition product (**3a**) is more stable with the dative hydride ligand on the outside of the wedge.

The addition of H_2S to imido complex **1** results in the formation of the sulfido complex **5**. One possible route to this compound involves formation of the S–H addition product analogous to **2** followed by elimination of H_2 (eq 3). However, we saw no evidence for an S–H addition product in the variable temperature ^{1}H NMR experiment, and addition of H_2 to the sulfido complex **5** yielded no reaction. We thought the toluamide complex **2** might also eliminate H_2, but heating a solution of **2** resulted in decomposition rather than formation of a bisimide complex.

The reaction of **1** with MeOTf to give **11** and methylcyclopentadiene is unexpected, especially when other potentially reactive ligands such as alkoxides or hydrides are available for reaction. The displacement of a Cp ligand by electrophiles from d_0 transition metals is unusual because the Cp ligand provides needed electron density to the electron deficient metal center.[66–69] Because they are more electron rich, many late transition metal complexes lose Cp easily or utilize it as an η^1 ligand.[66,70–77] the lengthening of the Ir–N bond and shortening of the Zr–N bond in **11** relative to complexes **2**, **3a**, and **9a** are an indication that the lone pair on nitrogen is partially donated to the zirconium center due to the lower electron density at zirconium caused by the loss of the Cp ligand.

The addition of phosphine to the O–H and N–H addition products is interesting from two perspectives. First, as discussed above, the 16-electron iridium center might be expected to coordinate phosphine. Second, previous work on Cp*Ir(NHPh)(H)(PPh$_3$) in our group suggested that the addition of phosphine might induce a reductive elimination of the imido and hydrido ligand from iridium.[59] the addition of ligands such as PPh$_3$, CO, and CH$_2$CH$_2$ to Cp*Ir(NHPh)(H)(PPh$_3$) has been shown to

(56) Dufour, N.; Majoral, J.; Caminade, A.; Choukroun, R.; Dromzée, Y. *Organometallics* **1991**, *10*, 45.
(57) Süss-Fink, G.; Pellinghelli, M. A.; Tiripicchio, A. *J. Organomet. Chem.* **1987**, *320*, 101.
(58) Arif, A. M.; Cowley, A. H.; Pakulski, M. *J. Am. Chem. Soc.* **1985**, *107*, 2553.
(59) Glueck, D. S.; Newman-Winslow, L. J.; Bergman, R. G. *Organometallics* **1991**, *10*, 1462.
(60) Cardin, D. J. *Chemistry of Organo-Zirconium and -Hafnium Compounds*; Wiley: New York, 1986; pp 98–103, 111–114.
(61) Erker, G. *Acc. Chem. Res.* **1984**, *17*, 103.
(62) Wolczanski, P. T.; Bercaw, J. E. *Acc. Chem. Res.* **1980**, *13*, 121.
(63) Ando, W.; Ohtaki, R.; Suzuki, T.; Kabe, Y. *J. Am. Chem. Soc.* **1991**, *113*, 7782.
(64) Parkin, G.; Bercaw, J. E. *J. Chem. Soc., Chem. Commun.* **1989**, 255.
(65) Tatsumi, K.; Nakamura, A.; Hofmann, P.; Stauffert, P.; Hoffmann, R. *J. Am. Chem. Soc.* **1985**, *107*, 4440.
(66) For a review of Cp ring slippage and substitution, see: O'Connor, J. M.; Casey, C. P. *Chem. Rev.* **1987**, *87*, 307.
(67) Lee, J. G.; Brubaker, C. H. *Inorg. Chim. Acta* **1977**, *87*, 307.
(68) Vitz, E.; Brubaker, C. H. *J. Organomet. Chem.* **1974**, *82*, C18.
(69) Peng, M. H.; Brubaker, C. H. *J. Organomet. Chem.* **1977**, *135*, 333.
(70) Werner, H.; Crisp, G. T.; Jolly, P. W.; Kraus, H. J.; Krüger, C. *Organometallics* **1983**, *2*, 1369.
(71) Werner, H. *J. Organomet. Chem.* **1980**, *200*, 335.
(72) Ryan, O. B.; TIlset, M.; Parker, V. D. *Organometallics* **1991**, *10*, 298.
(73) Paneque, M.; Maitlis, P. M. *J. Chem. Soc., Chem. Commun.* **1989**, 105.
(74) Jones, W. D.; Feher, F. J. *Organometallics* **1983**, *2*, 686.
(75) Anderson, G. K.; Cross, R. J.; Fallis, S.; Rocamora, M. *Organometallics* **1987**, *6*, 1440.
(76) Anderson, G. K. *Organometallics* **1986**, *5*, 1903.
(77) Hill, M. N. S.; Johnson, B. F. G.; Keating, R.; Lewis, J. *J. Chem. Soc., Dalton Trans.* **1975**, 1197.

result in the reductive elimination of H_2NPh and formation of Cp^*IrPPh_3L. When 2 equiv of PMe_3 were added to the *tert*-butyl alcohol addition product **3b**, $Cp_2Zr(NH\text{-}t\text{-}Bu)(O\text{-}t\text{-}Bu)$ (**12**) and $Cp^*Ir(PMe_3)_2$ were formed (Scheme 2). An intermediate observed in this reaction, displaying a new hydride resonance in the ^1H NMR spectrum and diastereotopic Cp ligands, could be assigned to the PMe_3 adduct **13**, isoelectronic to $Cp^*Ir(NHPh)(H)(L)$. Thus, the 16-electron iridium center coordinates phosphine to make a complex similar to the monomeric system. The ensuing reductive elimination reaction parallels those observed for $Cp^*Ir(NHPh)(H)(PPh_3)$. Addition of PPh_3 did not give a similar reaction, although the iridium systems previously studied coordinated PPh_3.[59] Neither the *p*-cresolate (**3a**) nor the *p*-toluamide (**2**) systems reacted productively with either PMe_3 or PPh_3. These three complexes differ only in the ligand on zirconium, yet the chemistry they exhibit is dramatically different. Changing the ligand on zirconium from *tert*-butoxide to *p*-cresolate or *p*-toluamide prevents the reductive elimination reaction which takes place at iridium.

The nonpolar reagents H_2 and $MePhSiH_2$ react reversibly with the metal–metal bond of imido complex **1**. It is not surprising that these products are less stable than the alcohol and amine addition products which contain strong Zr–O and Zr–N bonds.[78] The addition of a 1:1 mixture of H_2 and D_2 to imido complex **1** resulted in the formation of HD by ^1H NMR spectroscopy. One pathway for exchange involves a σ-bond metathesis reaction of D_2 with the hydride at zirconium.[79–83] An open coordination site at zirconium could be formed by dissociation of the bridging hydride ligand. Since the two hydrides of **9a** were shown to exchange with each other at room temperature, the label would quickly be incorporated into both positions. Alternatively, the exchange could take place at the iridium center via oxidative addition of D_2 to form an Ir(V) intermediate followed by reductive elimination of HD or by formation of a dideuterium complex followed by exchange and elimination of HD.[84–87] The exchange of deuterium into the Cp rings takes place at a rate comparable to the exchange of H_2 and D_2 to form HD, hence we could not determine whether the two processes were linked. Incorporation of deuterium into the Cp rings could occur directly from the dideuteride complex **9b**, or it could require the addition of 1 equiv of D_2.[81,88,89] We were unable to make the dideuteride complex **9b** without exchange of deuterium into the Cp rings during synthesis.

We felt that the presence of both iridium- and zirconium-bonded hydrides in **9a** might provide an opportunity for cooperative hydrogenation of unsaturated substrates. In agreement with this expectation, we observed the hydrogenation of ethylene, propylene, butene, 1-phenyl-1-propyne, 3-hexyne, and *N*-phenylbenzaldimine in the presence of imido complex **1**. However, dihydride **9a** did not cause the isomerization of 1-butene to 2-butene and did not hydrogenate 1-butene to *n*-butane. It was surprising that the butene isomerization process could not be catalyzed by the dihydride **9a**, leading us to suspect that another complex was involved in the hydrogenation and isomerization reactions. We established that the catalyst could not be **9a** when we observed that added PMe_3 led to inhibition of the rate of hydrogenation, but no observable amount of an adduct between **9a** and PMe_3 could be seen by ^1H NMR spectroscopy. If **9a** were on the reaction pathway, it would have to form an observable complex with PMe_3 in order to produce rate retardation. We are forced to conclude that PMe_3 must be scavenging an undetectably small amount of a catalytically active impurity. In contrast to the PMe_3 experiment, the addition of Hg to the reaction mixture resulted in no change in the rate of the reaction. If the catalyst were heterogeneous, the formation of an amalgam with Hg would be expected to cause an inhibition of the reaction rate.[52]

Conclusion

We have synthesized an early–late bridging imido complex (**1**) which displays cooperative reactivity with a wide range of organic substrates containing X–H bonds. Complex **1** is more reactive than previously synthesized complexes because both metal centers are coordinatively unsaturated, the complex possesses a reactive metal–metal bond, and the complex is linked by a relatively unreactive imido ligand. Imido complex **1** reacts with *tert*-butyl alcohol, *p*-cresol, *p*-toluidine, and acetone to make compounds with strong Zr–N and Zr–O bonds. However, it reacts with phosphines to make complexes with an Ir–P bond via an unusual phosphide insertion. We have also examined the reactivity of the products of the X–H addition reactions which do not contain Ir–Zr bonds. The addition of phosphines to the *p*-toluamide (**2**), *p*-cresolate (**3a**), and *tert*-butoxide (**3b**) complexes displayed a strong dependence on the nature of the ligand on zirconium, even though the overall process involves a reductive elimination reaction taking place at iridium. The addition of H_2 to imido complex **1** resulted in the formation of a dihydride containing both an early and late metal hydride in the same molecule. Although we observed the hydrogenation of unsaturated organic molecules with **1**, we found that the actual catalyst must be another compound present in small quantities in the reaction mixture. These results point out the hazards of assuming, in catalytic studies, that an NMR-observable organometallic complex present in solution is necessarily the active catalyst or catalyst precursor.

Experimental Section

General. Unless otherwise noted, all manipulations were carried out under an inert atmosphere in a Vacuum Atmospheres 553-2 drybox with attached MO-40-2 Dritrain or by using standard Schlenk or vacuum line techniques. Solutions were degassed by sequentially freezing to −196 °C, evacuating under high vacuum, and thawing. This sequence was repeated three times in each case. Glass reaction vessels fitted with ground glass joints and Teflon stopcocks are referred to as bombs.

^1H NMR spectra were obtained on either the 250-, 300-, 400-, or 500-MHz Fourier transform spectrometers at the University of California, Berkeley (UCB) NMR facility. The 250- and 300-MHz instruments were constructed by Mr. Rudi Nunlist and interfaced with either a Nicolet 1180 or 1280 computer. The 400- and 500-MHz instruments were commercial Bruker AM series spectrometers. Two additional (300 and 400 MHz) instruments were commercial Bruker AMX series spectrometers.

IR spectra were obtained on a Nicolet 510 FT-IR spectrometer or a Mattson Galaxy series FT-IR 3000 spectrometer. Mass spectroscopic (MS) analyses were obtained at the UCB mass spectrometry facility on AEI MS-12 and Kratos MS-50 mass spectrometers. Elemental analyses were obtained from the UCB Microanalytical Laboratory and Oneida Research Services. GC analyses were performed on a HP 5890A gas chromatograph equipped with a 95:5 dimethylsilicone:phenylmethylsilicone (DB5) column. The column was 30 m long, 0.25 mm in diameter, and made of fused silica. GCMS spectra were obtained on a HP 5970 series mass selective detector attached to a HP 5890A GC instrument. Sealed NMR tubes were prepared using Wilmad 505-PP and 504-PP tubes attached via Cajon adapters directly to Kontes vacuum stopcocks

(78) Schock, L. E.; Marks, T. J. *J. Am. Chem. Soc.* **1988**, *110*, 7701.
(79) Gell, K. I.; Schwartz, J. *J. Am. Chem. Soc.* **1978**, *100*, 3246.
(80) Gell, K. I.; Posin, B.; Schwartz, J.; Williams, G. M. *J. Am. Chem. Soc.* **1982**, *104*, 1846.
(81) Guo, Z.; Bradley, P. K.; Jordan, R. F. *Organometallics* **1992**, *11*, 2690.
(82) Lin, Z.; Marks, T. J. *J. Am. Chem. Soc.* **1987**, *109*, 7979.
(83) Thompson, M. E.; Baxter, S. M.; Bulls, A. R.; Burger, B. J.; Nolan, M. C.; Santarsiero, B. D.; Shaefer, W. P.; Bercaw, J. E. *J. Am. Chem. Soc.* **1987**, *109*, 203.
(84) Heinekey, D. M.; Millar, J. M.; Koetzle, T. F.; Payne, N. G.; Zilm, K. W. *J. Am. Chem. Soc.* **1990**, *112*, 909.
(85) Albeniz, A. C.; Heinekey, D. M.; Crabtree, R. H. *Inorg. Chem.* **1991**, *30*, 3632.
(86) Jessop, P. G.; Morris, R. H. *Inorg. Chem.* **1993**, *32*, 2236.
(87) Mediati, M.; Tachibana, G. N.; Jensen, C. M. *Inorg. Chem.* **1992**, *31*, 1827.
(88) Wochner, F.; Brintzinger, H. H. *J. Organomet. Chem.* **1986**, *309*, 65.
(89) McAlister, D. R.; Erwin, D. K.; Bercaw, J. E. *J. Am. Chem. Soc.* **1978**, *100*, 5966.

and degassed using freeze–pump–thaw cycles before flame sealing. Known volume bulb vacuum transfers were accomplished with an MKS baratron gauge attached to a high-vacuum line.

Unless otherwise specified, all reagents were purchased from commercial suppliers and used without further purification. $MePhSiH_2$ was distilled and stored over 4-Å sieves. *tert*-Butyl alcohol was dried sequentially over $MgSO_4$ and 4-Å sieves. Acetone was dried sequentially over $CaSO_4$ and 4-Å sieves. Pentane and hexanes (UV grade, alkene free) were distilled from sodium benzophenone ketyl/tetraglyme under nitrogen. Benzene, toluene, diethyl ether, and THF were distilled from sodium benzophenone ketyl under nitrogen. Deuterated solvents for use in NMR experiments were dried as their protiated analogs but were vacuum transferred from the drying agent. Cp*IrN-*t*-Bu[90] and $Cp_2Zr(N\text{-}t\text{-}Bu)(THF)$[91] were prepared by literature methods.

$Cp_2Zr(\mu\text{-}N\text{-}t\text{-}Bu)IrCp^*$ (1). To a solution of Cp_2ZrCl_2 (354 mg, 1.21×10^{-3} mol) in 10 mL of THF was added 1.50 mL of a 1.6 M solution of *n*-BuLi in hexanes (2.40×10^{-3} mol, 2 equiv) via syringe at −30 °C. The solution turned yellow. A solution of Cp*Ir-N-*t*-Bu (483 mg, 1.21×10^{-3} mol) in 1 mL of THF at −30 °C was immediately added to the reaction mixture. After warming to 25 °C, the solution was allowed to stand for 2 days. The solvent was removed under reduced pressure and the resulting brown solid suspended in 30 mL of diethyl ether. The LiCl was removed by filtration, after which the volume of the filtrate was reduced *in vacuo* to 20 mL and cooled to −30 °C. Dark brown microcrystals were obtained in two crops (491 mg, 7.93×10^{-4} mol, 65%): ^1H NMR (C_6D_6) δ 6.21 (s, 10H), 1.84 (s, 15H), 1.10 (s, 9H); $^{13}C\{^1H\}$ NMR (C_6D_6) δ 110.8 (s), 86.6 (s), 72.2 (s), 32.9 (s), 11.3 (s); IR (C_6D_6) 3049 (m), 2956 (s), 2900 (s), 2852 (m), 1373 (m), 1345 (m), 1009 (m), 921 (w), 775 (s) cm^{-1}, HRMS (EI) *m/e* calcd for $C_{24}H_{34}IrNZr$ 619.1368/617.1344 (M^+, $^{193}Ir/^{191}Ir$); *m/e* found 619.1384/617.1350 (M^+, $^{193}Ir/^{191}Ir$).

Crystal Structure Determination of 1. Dark brown block-like crystals of **1** were obtained by slow cooling of a diethyl ether solution to −30 °C. One of these crystals was mounted on a glass fiber using Paratone N hydrocarbon oil. The crystal was then transferred to an Enraf–Nonius CAD-4 diffractometer and centered in the beam. It was cooled to −110 °C by a nitrogen flow low-temperature apparatus, which had been previously calibrated by a thermocouple placed at the sample position. The final cell parameters and specific data collection parameters for this data set are given in Tables 1 and 2. The 1666 raw intensity data were converted to structure factor amplitudes and their esd's by correction for scan speed, background, and Lorentz and polarization effects. Inspection of the intensity standards revealed a reduction of 1.1% of the original intensity. The data were corrected for this decay. Space group *Cc* was confirmed by refinement. The structure was solved by Patterson methods and refined via standard least-squares and Fourier techniques. Inspection of the azimuthal scan data showed a variation of $I_{min}/I_{max} = 0.558$. An empirical absorption correction based on the differences of F_{obs} and F_{calc} after refinement of all atoms with isotropic thermal parameters was applied to the data. The final residuals for 117 variables refined against the 1425 data set for which $F^2 > 3\sigma(F^2)$ were $R = 3.1\%$, $R_w = 3.9\%$, and GOF = 1.86. The *R* value for all 1498 data was 3.3%. The largest peak in the final difference Fourier map had an electron density of 1.23 e^-/A^3 and the lowest excursion −0.38 e^-/A^3. The quantity minimized by the least-squares program was $\sum[w(|F_o| - |F_c|)^2]$, where *w* is the weight of a given observation. The *p*-factor, used to reduce the weight of intense reflections, was set to 0.03 in the last cycles of refinement. The analytical forms of the scattering factor tables for the neutral atoms were used, and all scattering factors were corrected for both the real and imaginary components of anomalous dispersion.

$Cp_2Zr(p\text{-}CH_3C_6H_4NH)(\mu\text{-}H)(\mu\text{-}N\text{-}t\text{-}Bu)IrCp^*$ (2). A solution of 16.5 mg of *p*-toluidine (1.54×10^{-4} mol, 1.1 equiv) in 1 mL of toluene was added to a solution of 90.4 mg of $Cp_2Zr(\mu\text{-}N\text{-}t\text{-}Bu)IrCp^*$ (**1**) (1.46×10^{-4} mol) in 5 mL of toluene. Immediately, the solution changed from dark brown to dark red. After 5 min, the volume of the solution was reduced *in vacuo* to 2 mL, layered with 0.5 mL of pentane, and cooled to −30 °C. Dark red crystals were isolated by decanting the solution. The crystals were crushed, washed with 3 × 1 mL of pentane to remove residual toluene, and dried *in vacuo* to provide 63.7 mg of **2** (8.76×10^{-5} mol, 60%): ^1H NMR (THF-d_8, −40 °C) δ 6.74 (d, $J = 7.6$ Hz, 2H), 6.34 (d, $J = 8.0$ Hz, 2H), 5.91 (s, 10H), 4.72 (s, 1H), 2.15 (s, 3H), 1.96 (s, 15H), 1.62 (s, 9H), −5.47 (s, 1H); $^{13}C\{^1H\}$ (toluene-d_8, −15 °C) δ 157.9 (s), 129.8 (s), 120.3 (s), 116.3 (s), 110.1 (s), 89.4 (s), 75.7 (s), 34.6 (s), 21.1 (s), 11.3 (s); IR (Nujol) 3072 (w), 2995 (m), 2878 (m), 2732 (m), 2096 (w), 1600 (s), 1503 (s), 1445 (s), 1285 (s), 1173 (s), 1027 (s), 794 (s), 764 (s), 721 (m), 497 (m) cm^{-1}. Anal. Calcd for $C_{31}H_{43}IrN_2Zr$: C, 51.20; H, 5.96; N, 3.85. Found: C, 51.16; H, 5.96; N, 4.10.

Crystal Structure Determination for 2. Clear red block-like crystals of **2** were obtained by slow cooling of a toluene solution to −30 °C and were mounted as described for **1**. X-ray data were collected as for **1**; the final cell parameters and specific data collection parameters for this data set are given in Tables 1 and 2.

Inspection of the intensity standards revealed a reduction of 3.9% of the original intensity. The data were corrected for this decay. Inspection of the azimuthal scan data showed a variation $I_{min}/I_{max} = 0.86$ for the average curve. An empirical correction based on the observed variation was applied to the data.

The structure was solved by Patterson methods and refined via standard least-squares and Fourier techniques. In a difference Fourier map calculated following the refinement of all non-hydrogen atoms with anisotropic thermal parameters, peaks were found corresponding to the positions of most of the hydrogen atoms. Hydrogen atoms were assigned idealized locations and values of B_{iso} approximately 1.3 times the B_{eqv} of the atoms to which they were attached. Hydrogens on the toluamide methyl groups were calculated in two possible positions and given half-occupancy. These hydrogens were included in structure factor calculations, but not refined. In a subsequent difference Fourier map, two peaks were located, one of which appeared to be the hydrogen on the nitrogen of the *p*-toluamide and the other of which appeared to be a bridging hydride. These were assigned fixed isotropic thermal parameters, and their positions were refined. Before the final cycles of refinement 15 reflections which were much higher than F_{calc}, apparently due to multiple diffraction, were given zero weight.

Inspection of the residuals ordered in ranges of $\sin(\theta)/\lambda$, $|F_o|$, and parity and value of the individual indexes showed no unusual features or trends. The largest peak in the final difference Fourier map had an electron density of 0.83 e^-/A^3 and the lowest excursion −0.24 e^-/A^3. Both were located near the iridium atom. There was no indication of secondary extinction in the high-intensity low-angle data.

$Cp_2Zr(p\text{-}CH_3C_6H_4O)(\mu\text{-}H)(\mu\text{-}N\text{-}t\text{-}Bu)IrCp^*$ (3a). To a solution of $Cp_2Zr(\mu\text{-}N\text{-}t\text{-}Bu)IrCp^*$ (**1**) (101 mg, 1.63×10^{-4} mol) in 5 mL of toluene was added a solution of *p*-cresol (18.1 mg, 1.67×10^{-4} mol) in 1 mL of toluene. Immediately, the solution turned dark red. After 5 min, the reaction mixture was filtered and the filtrate taken to dryness under reduced pressure. The product was crystallized from 3 mL of diethyl ether at −30 °C to provide red needles of **3a** (66.9 mg, 9.19×10^{-5} mol, 56%): ^1H NMR (C_6D_6) δ 7.26 (d, $J = 8.3$ Hz, 2H), 7.01 (d, $J = 8.3$ Hz, 2H), 6.03 (s, 10H), 2.37 (s, 3H), 1.593 (s, 15H), 1.588 (s, 9H), −7.24 (s, 1H); $^{13}C\{^1H\}$ NMR (C_6D_6) δ 164.7 (s), 130.4 (s), 125.2 (s), 119.0 (s), 110.8 (s), 88.3 (s), 73.4 (s), 32.1 (s), 20.9 (s), 11.4 (s); IR (Nujol) 3068 (w), 3007 (m), 2981 (m), 2878 (m), 2843 (m), 2728 (w), 2581 (w), 2357 (w), 2228 (w), 2164 (w), 1979 (m), 1600 (s), 1501 (s), 1432 (s), 1372 (s), 1342 (s), 1286 (s), 1183 (s), 1161 (s), 1023 (s), 1006 (s), 873 (s), 782 (s), 714 (s), 524 (s) cm^{-1}. Anal. Calcd for $C_{31}H_{42}IrNOZr$: C, 51.13; H, 5.81; N, 1.92. Found: C, 51.02; H, 5.73; N, 1.89.

Crystal Structure Determination of 3a. Small red blade-like crystals of **3a** were obtained by slow cooling of a 3:1 mixture of diethyl ether and hexamethyldisiloxane from reflux to 25 °C and were mounted as described for **1**. X-ray data were collected as for **1**; the final cell parameters and specific data collection parameters for this data set are given in Tables 1 and 2.

No correction for crystal decomposition was necessary. Inspection of the azimuthal scan data showed a variation $I_{min}/I_{max} = 0.76$ for the average curve. An empirical absorption correction based on the differences of F_{obs} and F_{calc} after refinement of all atoms with isotropic thermal parameters was applied to the data ($T_{max} = 1.087$, $T_{min} = 0.855$, used by the program DIFABS in MolEN).

The structure was solved by Patterson methods and refined via standard least-squares and Fourier techniques. The enantiomer of the structure was tested by refinement, and the reported enantiomer had a significantly lower residual. In a difference Fourier map calculated following the refinement of all non-hydrogen atoms with anisotropic thermal parameters, peaks were found corresponding to the positions of many of the hydrogen atoms. Hydrogen atoms of the ligands were assigned idealized locations and values of B_{iso} approximately 1.2 times the B_{eqv} of the atoms to which they were attached. They were included in structure factor calculations,

(90) Glueck, D. S.; Wu, J.; Hollander, F. J.; Bergman, R. G. *J. Am. Chem. Soc.* **1991**, *113*, 2041.

(91) Walsh, P. J.; Hollander, F. J.; Bergman, R. G. *Organometallics* **1993**, *12*, 3705.

but not refined. A peak in the correct position to be the missing hydride hydrogen was located in a subsequent difference Fourier map and was also included.

The largest peak in the final difference Fourier map had an electron density of 1.02 $e^-/Å^3$ and the lowest excursion −0.35 $e^-/Å^3$. There was no indication of secondary extinction in the high-intensity low-angle data.

$Cp_2Zr(Ot\text{-}Bu)(\mu\text{-}H)(\mu\text{-}N\text{-}t\text{-}Bu)IrCp^*$ (3b). To a solution of $Cp_2Zr(\mu\text{-}N\text{-}t\text{-}Bu)IrCp^*$ (**1**) (148 mg, 2.39×10^{-4} mol) in 5 mL of diethyl ether was added a solution of *tert*-butyl alcohol (18.6 mg, 2.51×10^{-4} mol) in 1 mL of diethyl ether. The reaction mixture immediately turned dark red. After 5 min, the volume of the solution was reduced to 1 mL *in vacuo*. Cooling the solution to −30 °C resulted in the formation of red needles, which were isolated by decanting the solvent and drying *in vacuo* to give 123 mg of **3b** (1.77×10^{-4} mol, 74%): ^1H NMR (C_6D_6) δ 6.11 (s, 10H), 1.63 (s, 15H), 1.54 (s, 9H), 1.41 (s, 9H), −6.03 (s, 1H); $^{13}C\{^1H\}$ NMR (C_6D_6) δ 111.6 (s), 88.1 (s), 77.1 (s), 72.6 (s), 32.8 (s), 32.7 (s), 11.6 (s); IR (Nujol) 3107 (w), 3091 (w), 2984 (m), 2925 (m), 2881 (m), 2837 (m), 2024 (m), 1770 (w), 1663 (w), 1555 (m), 1500 (s), 1472 (s), 1440 (s), 1373 (s), 1349 (s), 1182 (s), 1012 (s), 980 (s), 777 (s), 714 (s), 507 (s) cm^{-1}. Anal. Calcd for $C_{28}H_{44}IrNOZr$: C, 48.45; H, 6.39; N, 2.02. Found: C, 48.35; H, 6.25; N, 1.99.

$Cp_2Zr(OC(CH_2)(CH_3))(\mu\text{-}N\text{-}t\text{-}Bu)(\mu\text{-}H)IrCp^*$ (4). To a solution of $Cp_2Zr(\mu\text{-}N\text{-}t\text{-}Bu)IrCp^*$ (**1**) (89.7 mg, 1.45×10^{-4} mol) in 5 mL of toluene was added acetone (11.0 μL, 1.50×10^{-4} mol) via syringe. The solution was allowed to stir at 25 °C for 3 h, over which time it turned from brown to dark red. The volatile materials were removed under reduced pressure, and the resulting product was brought up in 20 mL of pentane and filtered. The volume of the filtrate was reduced to 10 mL *in vacuo*, and the solution was cooled to −30 °C. Red flakes of **4** were isolated by decanting the solvent and were dried under reduced pressure (70.3 mg, 1.04×10^{-4} mol, 72%): ^1H NMR (C_6D_6) δ 6.08 (s, 10H), 4.14 (s, 1H), 4.07 (d, J = 0.92 Hz, 1H), 2.05 (s, 3H), 1.59 (s, 15H), 1.55 (s, 9H), −7.29 (s, 1H); $^{13}C\{^1H\}$ NMR (C_6D_6) δ 166.2 (s), 116.7 (s), 88.2 (s), 83.7 (s), 73.3 (s), 32.1 (s), 24.9 (s), 11.4 (s); IR (Nujol) 3098 (m), 2984 (m), 2897 (m), 2719 (w), 2216 (w), 1974 (m), 1692 (w), 1605 (s), 1503 (m), 1477 (m), 1423 (m), 1356 (m), 1281 (s), 1184 (s), 1030 (s), 983 (m), 858 (m), 806 (s), 793 (s), 753 (s), 709 (s), 500 (s), 476 (m) cm^{-1}. Anal. Calcd for $C_{27}H_{40}IrNOZr$: C, 47.83; H, 5.95; N, 2.07. Found: C, 47.47; H, 6.04; N, 2.04.

$Cp_2Zr(p\text{-}CH_3C_6H_4S)(\mu\text{-}H)(\mu\text{-}N\text{-}t\text{-}Bu)IrCp^*$ (5a, 5b). To a solution of $Cp_2Zr(\mu\text{-}N\text{-}t\text{-}Bu)IrCp^*$ (**1**) (87.7 mg, 1.42×10^{-4} mol) in 3 mL of toluene was added a solution of *p*-thiocresol (17.6 mg, 1.42×10^{-4} mol) in 1 mL of toluene. The reaction mixture immediately turned from dark brown to dark red. The volume of the solution was reduced to 2 mL under reduced pressure. The solution was layered with 0.5 mL of pentane and cooled to −30 °C to produce red crystals of **5a** and **5b**, which were isolated by decanting the solvent and were dried *in vacuo* (67.1 mg, 9.02 × 10^{-5} mol, 64%). ^1H NMR and ^{13}C NMR data are given for major product **5a**: ^1H NMR (C_6D_6) δ 7.89 (d, J = 8.1 Hz, 2H), 7.08 (d, J = 7.8 Hz, 2H), 5.85 (s, 10H), 2.25 (s, 3H), 1.70 (s, 15H), 1.50 (s, 9H), −3.93 (s, 1H); $^{13}C\{^1H\}$ NMR (C_6D_6) δ 147.9 (s), 133.0 (s), 131.1 (s), 128.7 (s), 110.0 (s), 90.0 (s), 74.7 (s), 34.8 (s), 21.0 (s), 11.3 (s); IR (Nujol) 2994 (m), 2875 (m), 2724 (m), 1974 (w), 1787 (w), 1695 (w), 1595 (m), 1476 (s), 1439 (s), 1375 (s), 1343 (s), 1343 (s), 1169 (s), 1078 (s), 1014 (s), 804 (s), 707 (s), 625 (s), 497 (s) cm^{-1}. Combustion analysis was performed on the mixture of **5a** and **5b**. Anal. Calcd for $C_{28}H_{44}IrNOZr$: C, 50.03; H, 5.69; N, 1.88. Found: C, 49.82; H, 5.52; N, 1.59.

$Cp_2Zr(\mu\text{-}N\text{-}t\text{-}Bu)(\mu\text{-}S)IrCp^*$ from H_2S (6). An NMR tube was loaded with $Cp_2Zr(\mu\text{-}N\text{-}t\text{-}Bu)IrCp^*$ (**1**) (31.0 mg, 5.01×10^{-5} mol) and 0.6 mL of C_6D_6. The solution was degassed, and a known volume of H_2S (42 Torr, 23.5 mL, 5.3×10^{-5} mol) was condensed into the tube at −196 °C. The solution turned from dark brown to dark green upon thawing. All spectral data were obtained with this reaction mixture. In a separate experiment the yield of the reaction was determined by integration against an internal standard. An NMR tube was loaded with $Cp_2Zr(\mu\text{-}N\text{-}t\text{-}Bu)IrCp^*$ (**1**) (7.6 mg, 1.2×10^{-5} mol), *p*-dimethoxybenzene (1.2 mg, 8.7×10^{-6} mol), and 0.6 mL of C_6D_6. Two one-scan ^1H NMR spectra were taken. Then the solution was degassed and a known volume of H_2S (8.7 Torr, 23.5 mL, 1.1×10^{-5} mol) was condensed into the tube at −196 °C. The yield of the reaction was determined to be 45% by integration of the product against the internal standard: ^1H NMR (C_6D_6) δ 5.75 (s, 10H), 1.69 (s, 9H), 1.47 (s, 15H); $^{13}C\{^1H\}$ NMR (C_6D_6) δ 109.2 (s), 89.0 (s), 71.6 (s), 35.4 (s), 11.0 (s) (lit.[23] ^1H NMR (C_6D_6) δ 5.74 (s, 10H), 1.69 (s, 9H), 1.47 (s, 15H); $^{13}C\{^1H\}$ NMR (C_6D_6) δ 109.2 (s), 88.9 (s), 71.6 (s), 35.4 (s), 11.0 (s)).

$Cp_2Zr(\mu\text{-}t\text{-}BuNPEt_2)Ir(Cp^*)(H)$ (8a). A glass bomb was loaded with a solution of $Cp_2Zr(\mu\text{-}N\text{-}t\text{-}Bu)IrCp^*$ (**1**) (100 mg, 1.62×10^{-4} mol) in 20 mL of benzene. The solution was degassed, and a known volume of diethylphosphine (48 Torr in 66 mL, 1.7×10^{-4} mol) was condensed into the NMR tube at −196 °C. The solution turned dark red upon thawing. The benzene was removed from the reaction mixture under reduced pressure and the product crystallized from 5 mL of diethyl ether at −30 °C to give red needles of **8a** (72.3 mg, 1.02×10^{-4} mol, 63%): ^1H NMR (THF-d_8, −40 °C) δ 6.160 (s, 5H), 6.156 (s, 10H), 2.22 (m, 1H), 2.04 (s, 15H), 1.89 (m, 1H), 1.47 (m, 1H), 1.17 (m, 13H), 0.98 (dt, J = 18.1 Hz, J = 7.5 Hz, 3H), −14.16 (d, J = 29.3 Hz, 1H); $^{13}C\{^1H\}$ NMR (THF-d_8, −40 °C) δ 110.5 (s), 110.3 (s), 93.8 (d, J = 2.4 Hz), 56.2 (d, J = 11.3 Hz), 34.0 (d, J = 5.4 Hz), 29.3 (d, J = 33.3 Hz), 28.3 (d, J = 39.1 Hz), 11.5 (s), 11.1 (d, J = 1.5 Hz), 9.4 (s); $^{31}P\{^1H\}$ NMR (THF-d_8, 25 °C) δ −0.39; IR (Nujol) 2980 (m), 2921 (w), 2875 (w), 2815 (w), 2212 (m), 1439 (m), 1370 (m), 1352 (m), 1256 (m), 1178 (m), 1014 (s), 808 (s), 785 (s), 758 (s), 662 (m) cm^{-1}. Anal. Calcd for $C_{28}H_{45}IrNPZr$: C, 47.36; H, 6.39; N, 1.97. Found: C, 47.05; H, 6.40; N, 1.93.

Crystal Structure Determination of 8a. Clear red plate-like crystals of **8a** were obtained by slow cooling of a diethyl ether solution to −30 °C and were mounted as described for **1**. X-ray data were collected as described for **1**, and the final cell parameters and specific data collection parameters for this data set are given in Tables 7 and 8.

Inspection of the intensity standards revealed a reduction of 3.6% of the original intensity. The data were corrected for this decay. Inspection of the azimuthal scan data showed a variation I_{min}/I_{max} = 0.76 for the average curve. An empirical correction based on the observed variation was applied to the data.

The structure was solved by Patterson methods and refined via standard least-squares and Fourier techniques. In a difference Fourier map calculated following the refinement of all non-hydrogen atoms with anisotropic thermal parameters, peaks were found corresponding to the positions of all of the hydrogen atoms. Hydrogen atom positions were refined with isotropic thermal parameters in least-squares. In the final cycles of least-squares 13 data with abnormally large weighted difference values were given zero weight. (These were all in one region of reciprocal space and had larger than usual values for the background.) In the final cycles of refinement a secondary extinction parameter was included (maximum correction: 15% on F).

The largest peak in the final difference Fourier map had an electron density of 0.95 $e^-/Å^3$ and the lowest excursion −0.17 $e^-/Å^3$. The large positive peaks were located near the metal atoms.

$Cp_2Zr(\mu\text{-}t\text{-}BuNPCyH)Ir(Cp^*)(H)$ (8b). A glass bomb was loaded with $Cp_2Zr(\mu\text{-}N\text{-}t\text{-}Bu)IrCp^*$ (**1**) (175 mg, 2.82×10^{-4} mol), cyclohexylphosphine (41.1 μL, 3.10×10^{-4} mol, 1.1 equiv), and 5 mL of benzene. The solution was degassed and then heated to 80 °C overnight. The volatile materials were removed under reduced pressure, and the product was crystallized from 4 mL of toluene layered with 1 mL of pentane at −30 °C. Red crystals of **8b** were isolated by decanting the solvent and were dried *in vacuo* (105 mg, 1.42×10^{-4} mol, 50%): ^1H NMR (THF-d_8) δ 6.21 (s, 5H), 6.29 (s, 5H), 5.14 (d, J = 349.3 Hz, 1H), 2.10 (s, 15H), 1.73 (m, 5H), 1.25 (m, 6H), 1.11 (s, 9H), −14.7 (d, J = 29.9 Hz, 1H); $^{13}C\{^1H\}$ NMR (THF-d_8) δ 110.6 (s), 110.1 (s), 94.1 (d, J = 2.3 Hz), 54.5 (d, J = 9.7 Hz), 36.4 (d, J = 42.3 Hz), 32.9 (d, J = 6.8 Hz), 30.1 (d, J = 2.3 Hz), 27.6 (d, J = 16.1 Hz), 27.5 (s), 26.6 (d, J = 13.9 Hz), 26.2 (d, J = 6.0 Hz), 11.5 (s); $^{31}P\{^1H\}$ NMR (C_6D_6) δ −14.9; IR (Nujol) 2990 (m), 2878 (m), 2844 (m), 2207 (s), 1445 (m), 1357 (m), 1192 (s), 1017 (s), 901 (s), 871 (s), 784 (s), 745 (s), 561 (m), 488 (m); HRMS (EI) m/e calcd for $C_{30}H_{47}IrNPZr$ 735.2123/733.2099 (M^+, $^{193}Ir/^{191}Ir$); m/e found 735.2150/733.2113 (M^+, $^{193}Ir/^{191}Ir$).

$Cp_2Zr(H)(\mu\text{-}H)(\mu\text{-}N\text{-}t\text{-}Bu)IrCp^*$ (9a). A glass bomb was loaded with a solution of $Cp_2Zr(\mu\text{-}N\text{-}t\text{-}Bu)IrCp^*$ (**1**) (160 mg, 2.58×10^{-4} mol) in 10 mL of diethyl ether. The solution was degassed and then filled with 700 Torr of H_2. The solution was shaken and immediately turned bright red. The volume of the solution was reduced *in vacuo* to 5 mL and cooled to −30 °C. It was found to be very important not to remove all of the solvent from the reaction mixture to prevent decomposition. Red crystals of **9a** were isolated by decanting the diethyl ether and were dried *in vacuo* (111 mg, 1.79×10^{-4} mol, 69%): ^1H NMR (THF-d_8) δ 5.34 (s, 10H), 1.89 (s, 15H), 1.56 (s, 9H), −0.71 (d, J = 6.4 Hz, 1H), −1.95 (d, J = 6.2 Hz, 1H); $^{13}C\{^1H\}$ NMR (THF-d_8) δ 102.0 (s), 89.0 (s), 73.5 (s), 34.8 (s), 11.3 (s); IR (Nujol) 3085 (w), 2987 (m), 1986 (vw), 1477 (m), 1437 (m), 1381 (m), 1344 (m), 1181 (m), 1014 (s), 787 (s), 754 (s), 717 (m), 678 (s). Due to the sensitivity of **9a**, we were unable to obtain satisfactory combustion analysis or mass spectral data.

Crystal Structure Determination of 9a. Clear red crystals of **9a** were obtained by slow crystallization from diethyl ether at −30 °C and were mounted as described for **1**. X-ray data were collected as for **1**, and the

final cell parameters and specific data collection parameters for this data set are given in Tables 7 and 8.

No correction for crystal decomposition was performed, although the intensity standards varied during data collection. The averaging statistics showed that no corrections were necessary. Inspection of the azimuthal scan data showed a variation $I_{min}/I_{max} = 0.56$ for the average curve. However, there were clear indications that during the azimuthal scans at least some of the reflections were misoriented in the counting aperture. Therefore, an empirical correction based on the differences of F_{obs} and F_{calc} after refinement of all atoms with isotropic thermal parameters (using the unaveraged data) was applied to the data ($T_{max} = 1.33$, $T_{min} = 0.83$, used by the program DIFABS in MolEN). Inspection of the systematic absences indicated possible space groups *Pnma* and $Pn2_1a$. The choice of the centric group was confirmed by the successful solution and refinement of the structure. Removal of systematically absent data and averaging of redundant data ($R_I = 2.3\%$) left 3429 unique data in the final data set.

The structure was solved by Patterson methods in space group *Pnma* and refined via standard least-squares and Fourier techniques. In a difference Fourier map calculated following the refinement of all non-hydrogen atoms with anisotropic thermal parameters, peaks were found corresponding to the positions of most of the hydrogen atoms. Hydrogen atoms were assigned idealized locations and then were refined with isotropic thermal parameters. The hydride hydrogens were located on a subsequent difference Fourier map and refined similarly. In the final cycles of least-squares two data with abnormally large weighted difference values (apparently due to multiple diffraction) were given zero weight. In the final cycles of refinement a secondary extinction parameter was included (maximum correction: 8% on F).

The largest peak in the final difference Fourier map had an electron density of 0.94 $e^-/Å^3$ and the lowest excursion –0.22 $e^-/Å^3$. The large peaks were located near the Ir and Zr atoms.

$Cp_2Zr(D)(\mu\text{-}D)(\mu\text{-}N\text{-}t\text{-}Bu)IrCp^*$ (9b). A glass bomb was loaded with $Cp_2Zr(\mu\text{-}N\text{-}t\text{-}Bu)IrCp^*$ (**1**) (125 mg, 2.02×10^{-4} mol) and 20 mL of diethyl ether. The solution was degassed and filled with 700 Torr of D_2. The volume of the diethyl ether was reduced to 5 mL *in vacuo*, and the solution was cooled to –30 °C to produce red crystals of **9b** (78.6 mg, 1.26×10^{-4} mol, 63%). ^1H NMR and $^{13}C\{^1H\}$ NMR spectral data were the same as for **9a** above. ^2H NMR (C_6H_6): δ 5.48 (s), –0.23 (s), –1.81 (s).

$Cp_2Zr(Ph(Me)SiH)(\mu\text{-}H)(\mu\text{-}N\text{-}t\text{-}Bu)IrCp^*$ (10). An NMR tube was loaded with $Cp_2Zr(\mu\text{-}N\text{-}t\text{-}Bu)IrCp^*$ (**1**) (23.2 mg, 3.75×10^{-5} mol), methylphenylsilane (35 μL, 2.5×10^{-4} mol, 7 equiv), and 0.6 mL of THF-d_8. The solution turned immediately from dark brown to bright red. Due to the instability of **10**, all spectral data were obtained with this reaction mixture. In a separate experiment, the yield of the reaction was determined by integration against an internal standard. An NMR tube was loaded with $Cp_2Zr(\mu\text{-}N\text{-}t\text{-}Bu)IrCp^*$ (**1**) (8.2 mg, 1.3×10^{-5} mol), *p*-dimethoxybenzene (1.4 mg, 1.0×10^{-5} mol), and 0.6 mL of C_6D_6. Two one-scan ^1H NMR spectra were taken. Then methylphenylsilane (12.7 μL, 9.24×10^{-5} mol, 7 equiv) was added to the NMR tube and the yield determined by integration of the product against *p*-dimethoxybenzene. The yield of **10** was determined to be 94%: ^1H NMR (THF-d_8) δ 7.69 (dm, $J = 6.6$ Hz, 2H), 7.25 (tm, $J = 7.1$ Hz, 2H), 7.18 (tm, $J = 7.2$ Hz, 1H), 5.50 (m, 1H), 5.47 (s, 5H), 5.30 (s, 5H), 1.88 (s, 15H), 1.67 (s, 9H), 0.74 (d, $J = 4$ Hz, 3H), –3.71 (s, 1H); $^{13}C\{^1H\}$ NMR (THF-d_8) δ 150.1 (s), 136.0 (s), 127.8 (s), 127.2 (s), 104.5 (s), 104.1 (s), 89.9 (s), 74.5 (s), 35.4 (s), 11.9 (s), 2.18 (s); IR (THF-d_8) 2971 (m), 2953 (m), 2901 (s), 2006 (m), 1666 (m), 1560 (m), 1444 (m), 1377 (m), 1348 (m), 1228 (m), 1201 (m), 807 (s) cm^{-1}.

$CpZr(O\text{-}t\text{-}Bu)(OS(O)_2(CF_3))(\mu\text{-}H)(\mu\text{-}N\text{-}t\text{-}Bu)IrCp^*$ (11). To a solution of $Cp_2Zr(O\text{-}t\text{-}Bu)(\mu\text{-}H)(\mu\text{-}N\text{-}t\text{-}Bu)IrCp^*$ (**3b**) (130 mg, 1.88×10^{-4} mol) in 5 mL of toluene was added methyl triflate (23.4 μL, 2.07×10^{-4} mol, 1.1 equiv). The reaction mixture was stirred for 2 days, over which time it turned red. The volatile materials were removed under reduced pressure, and the resulting red solid was dissolved in 5 mL of diethyl ether. The solution was filtered, and then the volume was reduced to 0.5 mL under reduced pressure. Hexamethyldisiloxane (0.1 mL) was added to the solution, and large crystals of **13** formed at 25 °C upon slow evaporation of the solvent (88.4 mg, 1.17×10^{-4} mol, 62%): ^1H NMR (C_6D_6) δ 6.34 (s, 5H), 1.56 (s, 15H), 1.39 (s, 9H), 1.25 (s, 9H), –5.33 (s, 1H); ^{13}C NMR (C_6D_6) δ 120.35 (q, $J = 318$ Hz), 112.8 (s), 90.5 (s), 79.8 (s), 70.3 (s), 33.4 (s), 32.0 (s), 11.0 (s); $^{19}F\{^1H\}$ (C_6D_6) δ –77.4; IR (Nujol) 3098 (m), 2987 (m), 2880 (m), 2837 (m), 2193 (w), 1950 (m), 1495 (m), 1473 (m), 1445 (m), 1382 (m), 1357 (m), 1337 (s), 1234 (s), 1186 (s), 1013 (s), 804 (s), 784 (s), 721 (s), 628 (s) cm^{-1}; IR (C_6D_6) 3045 (m), 2967 (m), 2914 (m), 2354 (w), 2325 (w), 2268 (w), 1943 (w), 1869 (w), 1384 (m), 1341 (m), 1236 (m), 1202 (s), 1180 (s), 1018 (s), 996 (s), 723 (m), 630 (m). Anal. Calcd for $C_{24}H_{39}F_3IrNO_4SZr$: C, 37.05; H, 5.05; N, 1.80. Found: C, 36.98; H, 4.72; N, 1.67.

Crystal Structure Determination of 11. Block-like red crystals of **11** were obtained by slow crystallization from a mixture of diethyl ether and hexamethyldisiloxane at 25 °C and were mounted as described for **1**. X-ray data were collected as for **1**, and the final cell parameters and specific data collection parameters for this data set are given in Tables 7 and 8.

Inspection of the intensity standards revealed a reduction of 4% of the original intensity. The data were corrected for this decay. Inspection of the azimuthal scan data showed a variation $I_{min}/I_{max} = 0.71$ for the average curve. An empirical correction based on the observed variation was applied to the data.

The structure was solved by Patterson methods and refined via standard least-squares and Fourier techniques. The cyclopentadienide ligand attached to the Zr was found to be severely disordered and was refined as two sets of half-occupancy carbon atoms. In a difference Fourier map calculated following the refinement of all undisordered non-hydrogen atoms with anisotropic thermal parameters, peaks were found corresponding to the positions of most of the hydrogen atoms. Hydrogen atoms for all but the Cp and the hydride were assigned idealized locations and values of B_{iso} approximately 1.25 times the B_{eqv} of the atoms to which they were attached. They were included in structure factor calculations, but not refined. In a subsequent difference Fourier map, a peak was found in a location suggesting that it was the bridging hydride. The hydride positional and isotropic thermal parameters were included in the refinement. In the final cycles of refinement a secondary extinction parameter was included (maximum correction: 5% on F).

The largest peak in the final difference Fourier map had an electron density of 1.67 $e^-/Å^3$ and the lowest excursion –0.22 $e^-/Å^3$.

Addition of MeOTf to $Cp_2Zr(O\text{-}t\text{-}Bu)(\mu\text{-}H)(\mu\text{-}N\text{-}t\text{-}Bu)IrCp^*$ (3b): Identification of Methylcyclopentadiene. To a solution of $Cp_2Zr(O\text{-}t\text{-}Bu)(\mu\text{-}H)(\mu\text{-}N\text{-}t\text{-}Bu)IrCp^*$ (**3b**) (15.7 mg, 2.26×10^{-5} mol) in 1 mL of diethyl ether was added methyl triflate (2.8 μL, 2.5×10^{-5} mol, 1.1 equiv). The reaction mixture was allowed to stir for 2 days at 25 °C, during which time it turned from brown to red and a slight precipitate formed. The reaction mixture was then removed from the drybox, and to it were added 1 mL of water and 5.0 μL of methylcyclohexane (3.9×10^{-5} mol). A 1-μL sample of the ethereal layer was injected onto the GC column. The yield of methylcyclopentadiene was determined to be 18% by integration against methylcyclohexane. The identity of methylcyclopentadiene was confirmed by coinjection with an authentic sample and by GCMS analysis. In a second experiment, an NMR tube was loaded with $Cp_2Zr(O\text{-}t\text{-}Bu)(\mu\text{-}H)(\mu\text{-}N\text{-}t\text{-}Bu)IrCp^*$ (**3b**) (10.5 mg, 1.51×10^{-5} mol), methyl triflate ($1.8\ \mu L$, 1.6×10^{-5} mol), and 0.6 mL of C_6D_6. The reaction mixture was degassed and was allowed to stand at 25 °C for 2 days. The NMR tube was opened, and the volatile materials were vacuum transferred into another NMR tube. Methylcyclopentadiene was identified by ^1H NMR spectroscopy as the only product by comparison to an authentic sample.

$Cp_2Zr(NH\text{-}t\text{-}Bu)(O\text{-}t\text{-}Bu)$ (12). $Cp_2Zr(N\text{-}t\text{-}Bu)(THF)$ (78.0 mg, 2.14×10^{-4} mol) was dissolved in 10 mL of benzene, and to it was immediately added a solution of *tert*-butyl alcohol (14.1 mg, 1.90×10^{-4} mol, 0.9 equiv) in 1 mL of benzene. The solution turned from pale yellow to colorless. The volatile materials were removed *in vacuo*, and the product was dissolved in 1 mL of pentane. Upon cooling to –30 °C white crystals of **11** formed (38.3 mg, 1.04×10^{-4} mol, 49%): ^1H NMR (C_6D_6) δ 5.93 (s, 10H), 3.50 (s, 1H), 1.24 (s, 9H), 1.13 (s, 9H); $^{13}C\{^1H\}$ δ 110.9 (s), 76.4 (s), 54.8 (s), 34.5 (s), 32.1 (s); IR (Nujol) 3332 (w), 3086 (m), 2978 (m), 2925 (w), 1354 (m), 1188 (s), 1013 (s), 969 (s), 723 (m), 782 (s); HRMS (EI) *m/e* calcd for $C_{18}H_{29}NOZr$ 365.1296 (M^+, ^{90}Zr); *m/e* found 365.1306 (M^+, ^{90}Zr).

Addition of Two Equivalents of PMe_3 to $Cp_2Zr(O\text{-}t\text{-}Bu)(\mu\text{-}H)(\mu\text{-}N\text{-}t\text{-}Bu)IrCp^*$ (3b). An NMR tube was loaded with $Cp_2Zr(O\text{-}t\text{-}Bu)(\mu\text{-}H)(\mu\text{-}N\text{-}t\text{-}Bu)IrCp^*$ (**3b**) (31.9 mg, 4.60×10^{-5} mol) and 0.6 mL of C_6D_6. The solution was degassed, and 73 Torr of PMe_3 in a 23.5-mL known volume bulb (9.2×10^{-4} mol, 2.0 equiv) was condensed into the reaction mixture at –196 °C. The reaction was allowed to stand at 25 °C for 1 day. All spectral data were obtained with this reaction mixture.

In a separate experiment, the yield of the reaction was determined by integration against an internal standard. An NMR tube was loaded with $Cp_2Zr(O\text{-}t\text{-}Bu)(\mu\text{-}H)(\mu\text{-}N\text{-}t\text{-}Bu)IrCp^*$ (**3b**) (9.2 mg, 1.3×10^{-5} mol), *p*-dimethoxybenzene (1.1 mg, 8.0×10^{-6} mol, 0.6 equiv), and 0.6 mL of C_6D_6. Two one-scan ^1H NMR spectra were taken. The solution was degassed and 21 Torr of PMe_3 in a 23.5-mL known volume bulb ($2.6 \times$

10^{-5} mol, 2.0 equiv) was condensed into the reaction mixture at −196 °C. The yield was determined by integration of the product peaks in the ^1H NMR spectrum relative to the internal standard. The yield of $Cp^*Ir(PMe_3)_2$ was 84%, and the yield of $Cp_2Zr(NH\text{-}t\text{-}Bu)(O\text{-}t\text{-}Bu)$ was 58%.

^1H NMR and $^{13}C\{^1H\}$ NMR spectral data for $Cp_2Zr(NH\text{-}t\text{-}Bu)(O\text{-}t\text{-}Bu)$ (**12**) were identical to those found in the independent synthesis reported above. Spectral data for $Cp^*Ir(PMe_3)_2$: ^1H NMR (C_6D_6) δ 2.06 (br s), 1.43 (d, J = 8.1 Hz); $^{13}C\{^1H\}$ (C_6D_6) δ 91.60 (br, s), 25.5 (five-line pattern), 12.40 (s); $^{31}P\{^1H\}$ (C_6D_6) δ −54.44 (lit.[51] ^1H NMR (C_6D_6) δ 2.07 (t, J = 1.0 Hz, 15H), 1.43 (d, $^2J_{HP} + {}^4J_{HP}$ = 8.7 Hz, 9H); $^{13}C\{^1H\}$ (C_6D_6) δ 91.62 (br s), 25.5 (five-line pattern), 12.39 (s); $^{31}P\{^1H\}$ (C_6D_6) δ −54.35).

Incorporation of D_2 into $Cp_2Zr(D)(\mu\text{-}D)(\mu\text{-}N\text{-}t\text{-}Bu)IrCp^*$ (9b). An NMR tube was loaded with $Cp_2Zr(\mu\text{-}N\text{-}t\text{-}Bu)IrCp^*$ (**1**) (17.2 mg, 2.78 × 10^{-5} mol) and 0.6 mL of benzene. The solution was degassed and filled with 650 Torr of D_2 at 77 K. The reaction was shaken and monitored by ^2H NMR. Incorporation of deuterium into the Cp resonances was found to reach equilibrium after 3 h.

Addition of H_2 and D_2 to $Cp_2Zr(\mu\text{-}N\text{-}t\text{-}Bu)IrCp^*$ (1) To Form HD. An NMR tube was charged with $Cp_2Zr(\mu\text{-}N\text{-}t\text{-}Bu)IrCp^*$ (**1**) (7.4 mg, 1.2 × 10^{-5} mol) and 0.6 mL of C_6D_6. The solution was degassed and filled with 350 Torr of H_2 and 350 Torr of D_2 at 77 K. The tube was flame sealed and shaken at 25 °C for 4 h. HD was observed by the appearance of its characteristic 1:1:1 triplet in the ^1H NMR spectrum (C_6D_6) at 4.42 ppm, J = 43 Hz.

Equilibration of $Cp_2Zr(H)(\mu\text{-}H)(\mu\text{-}N\text{-}t\text{-}Bu)IrCp^*$ (9a) and $Cp_2Zr(D)(\mu\text{-}D)(\mu\text{-}N\text{-}t\text{-}Bu)IrCp^*$ (9b). An NMR tube was charged with $Cp_2Zr(H)(\mu\text{-}H)(\mu\text{-}N\text{-}t\text{-}Bu)IrCp^*$ (**9a**) (4.7 mg, 7.6 × 10^{-5} mol), $Cp_2Zr(H)(\mu\text{-}H)(\mu\text{-}N\text{-}t\text{-}Bu)IrCp^*$ (**9b**) (4.8 mg, 7.7 × 10^{-5} mol), and 0.6 mL of C_6D_6. Complexes $Cp_2Zr(D)(\mu\text{-}H)(\mu\text{-}N\text{-}t\text{-}Bu)IrCp^*$ (**9c**) and $Cp_2Zr(H)(\mu\text{-}D)(\mu\text{-}N\text{-}t\text{-}Bu)IrCp^*$ (**9d**) were observed in the ^1H NMR spectrum after 1 h. The reaction was monitored after 6 h and found to have a similar ^1H NMR spectrum: ^1H NMR (C_6D_6) δ 5.50 (s), 1.69 (s), 1.58 (s), −0.26 (s), −1.81 (s). The dihydride $Cp_2Zr(H)(\mu\text{-}H)(\mu\text{-}N\text{-}t\text{-}Bu)IrCp^*$ (**9a**) was also observed in the ^1H NMR spectrum.

Removal of H_2 from $Cp_2Zr(H)(\mu\text{-}H)(\mu\text{-}N\text{-}t\text{-}Bu)IrCp^*$ (9a). An NMR tube was charged with $Cp_2Zr(\mu\text{-}N\text{-}t\text{-}Bu)IrCp^*$ (**1**) (7.2 mg, 1.2 × 10^{-5} mol) and 0.6 mL of C_6D_6. The solution was degassed, filled with 700 Torr of H_2 at 77 K, and then flame sealed. ^1H NMR spectroscopy showed the formation of $Cp_2Zr(H)(\mu\text{-}H)(\mu\text{-}N\text{-}t\text{-}Bu)IrCp^*$ (**9a**). The volatile materials were removed under reduced pressure, and the resulting solid was dissolved in 2 mL of toluene. The toluene and volatile materials were removed under reduced pressure, and the resulting solid was dissolved in 0.6 mL of C_6D_6 and loaded into an NMR tube. ^1H NMR spectroscopy showed 70% conversion to $Cp_2Zr(\mu\text{-}N\text{-}t\text{-}Bu)IrCp^*$ (**1**).

General Procedure for the Determination of Catalytic Hydrogenation Turnover Rates. The same general procedure was used for the hydrogenation reactions of $Cp_2Zr(\mu\text{-}N\text{-}t\text{-}Bu)IrCp^*$ (**1**) with ethylene, propylene, 1-butene, *cis*-2-butene, *trans*-2-butene, 3-hexyne, 1-phenyl-1-propyne, and *N*-phenylbenzaldimine. The reaction with ethylene is given below as an example of the general procedure. An NMR tube was charged with $Cp_2Zr(\mu\text{-}N\text{-}t\text{-}Bu)IrCp^*$ (**1**) (4.7 mg, 7.6 × 10^{-6} mol, 5 mol %) and 0.6 mL of C_6D_6. The solution was degassed, and ethylene (1.52 × 10^{-3} mol) was vacuum transferred into the tube. Then the tube was filled with 500 Torr of H_2 and flame sealed. The reaction was shaken at 25 °C and monitored by ^1H NMR spectroscopy. In the reaction with PMe_3, 5 equiv was added to the reaction mixture. In the reactions with Hg, 10 μL was added to the reaction mixture.

Acknowledgment. We are grateful to Dr. Frederick Hollander for solving the crystal structures of **1**, **2**, **3a**, **8a**, **9a**, and **11**, to Dr. Graham Ball for assistance with the NOESY and EXSY experiments, and to the NSF for support of this work, through Grant No. CHE-9113261. We also acknowledge a gift of iridium chloride from the Johnson–Matthey Aesar/Alfa metal loan program.

Supplementary Material Available: Additional structural data for complexes **1**, **2**, **3a**, **8a**, **9a**, and **11** (17 pages). This material is contained in many libraries on microfiche, immediately follows this article in the microfilm version of the journal, and can be ordered from the ACS; see any current masthead page for ordering information.